Chapter 4

Large elastic anomalies in C_{66}

In this chapter we will discuss on the large elastic softening in C_{66}. Fig 4.1 shows the T dependence of C_{66} for the samples with $x = 0$, 0.037, 0.060, 0.084, 0.098, 0.116, 0.161, and 0.245. C_{66} significantly decreases as T decreases. Although a decrease in elastic stiffness is a common feature of structural phase transition. The amount of softening, i.e., as much as 80% for $Ba(Fe_{0.963}Co_{0.037})_2As_2$, is unprecedentedly large. The softening in C_{66} corresponds to a symmetry change from tetragonal to orthorhombic. This is consistent with the result of the structural analysis of this material, where the space groups are $I4/mmm$ and $Fmmm$ for the high- and low-temperature phases, respectively.

The decrease in C_{66} with decreasing T is prominent for $x = 0$, 0.037, which follow the disappearance of the signal at structural transition temperatures $T_S = 141$K ($x = 0$), 84.7K ($x = 0.037$). The data below T_S were not plotted for $x = 0$ or 0.037, because the sound echo signal disappeared in a certain temperature range below T_S, which may be ascribed

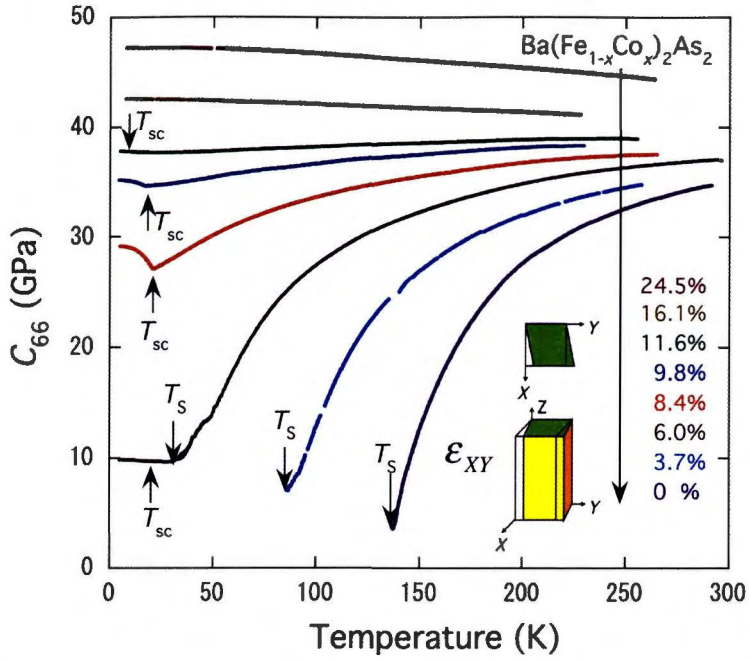

Figure 4.1: Temperature dependence of the elastic stiffness C_{66} of $Ba(Fe_{1-x}Co_x)_2As_2$ with various Co concentrations.

to strong scattering of the sound by orthorhombic domain boundaries. The softening of C_{66} is less prominent as x increases, which is consistent with the disappearance of the structural phase transition. For the superconducting samples, $0.060 \leq x \leq 0.116$ anomalies are observed at $T_{sc} = 24$ K ($x = 0.060$), 20.7 K ($x = 0.084$), 16.5 K ($x = 0.098$), and 10.5 K ($x = 0.116$).

The underdoped samples show a peak at T_{sc} and a steplike anomaly below T_{sc}. On the other hand, C_{66} increases below T_{sc} in the overdoped region. This difference will be discussed later. Moreover, the superconducting transition disappears when $x > 0.161$. The C_{66} values of the samples of $x = 0.161$ and 0.245 show gradual increases as T decreases, which a typical behavior for any material, reflecting phonon anharmonic-

ity.

4.1 Origin of C_{66} softening

4.1.1 Analysis based on localized picture

The observed large elastic anomaly in C_{66} is a precursor of structural phase transition. Here, we will discuss the origin of the softening in C_{66}. 3d orbitals are split into an E_g doublet and a T_{2g} triplet by an electric crystalline field (CEF) in a cubic symmetry. E_g is split into two singlets, and T_{2g} is split into one singlet and one doublet by the tetragonal CEF of iron-based materials. The remaining doublet can be lifted by the elastic strain and may cause elastic anomaly these description was seen in Fig. 4.2. We will consider the coupling between the strain ε and the order parameter O as $H = -\lambda O_\Gamma \varepsilon_\Gamma$. The equivalence of the X- and Y-axes

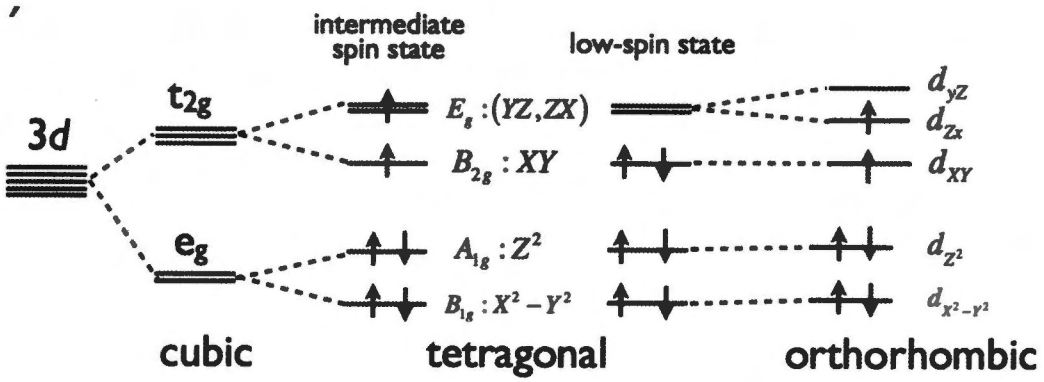

Figure 4.2: Schematic illustration of a ground state d6 configuration of Fe ion with an intermediate spin state of S = 1 and low-spin state.

in tetragonal symmetry leads to the degeneration of the d_{ZX} and d_{YZ} orbitals. This degeneracy is lifted by ε_{XY} or $\varepsilon_{XX} - \varepsilon_{YY}$, and brings

about anomalies in the corresponding C_{66} and $\frac{1}{2}(C_{11} - C_{12})$. The strain ε_{XY} can couple with the orbital (quadrupole) O_{XY}. We can calculate the strain susceptibility based on a localized picture of d electrons:

$$C_{66} = C_{66,0} - N\lambda^2 \frac{\chi^0_{66}}{1 - I\chi^0_{66}} = C_{66,0} \frac{T - T_C}{T - \Theta} \tag{4.1}$$

where λ, I and N are the coupling constant, intersite interaction, and number of atoms per unit volume. Here, we adopted the form $\chi^0_{66} =< (O_{XY})^2 > /T$ for localized d electrons. Here, we introduce the elastic compliance S_{ij}, which is a component of the inverse C_{ij} matrix. In eq. 4.1, the transition occurs at T_C, where the lattice shows instability. Elastic compliance represents the "structural" susceptibility of elastic systems, and corresponds to the magnetic susceptibility χ in magnetic systems. The experimentally observed S_{66} $(= \frac{1}{C_{66}})$ can be decomposed into the sum of the anomalous contributions that exhibit critical behavior, $S_{66,cr}$, and the normal contribution (background) $S_{66,0}$:

$$S_{66} = S^0_{66} + S_{66,cr} = S_{66,0}(1 + \frac{E_{JT}}{T - T_C}) \tag{4.2}$$

where $E_{JT} = T_C - \Theta$. E_{JT} stands for the JahnTeller energy, an energy scale that corresponds to the strength of the electron-lattice coupling. Note that this formula has the same form as the CurieWeiss susceptibility of ferromagnetic materials.

For the analysis, we employed the data of $Ba(Fe_{0.755}Co_{0.245})_2As_2$ for $S_{66,0}$, and subtract it from the other data. Figure 4.3 shows the inverse

of $S_{66,cr}$ as a function of temperature. It can clearly be seen that $1/S_{66,cr}$ in the underdoped region ($x < 0.070$) exhibits a linear T dependence. This indicates that $S_{66,cr}$ obeys eq. 4.2. In the underdoped samples,

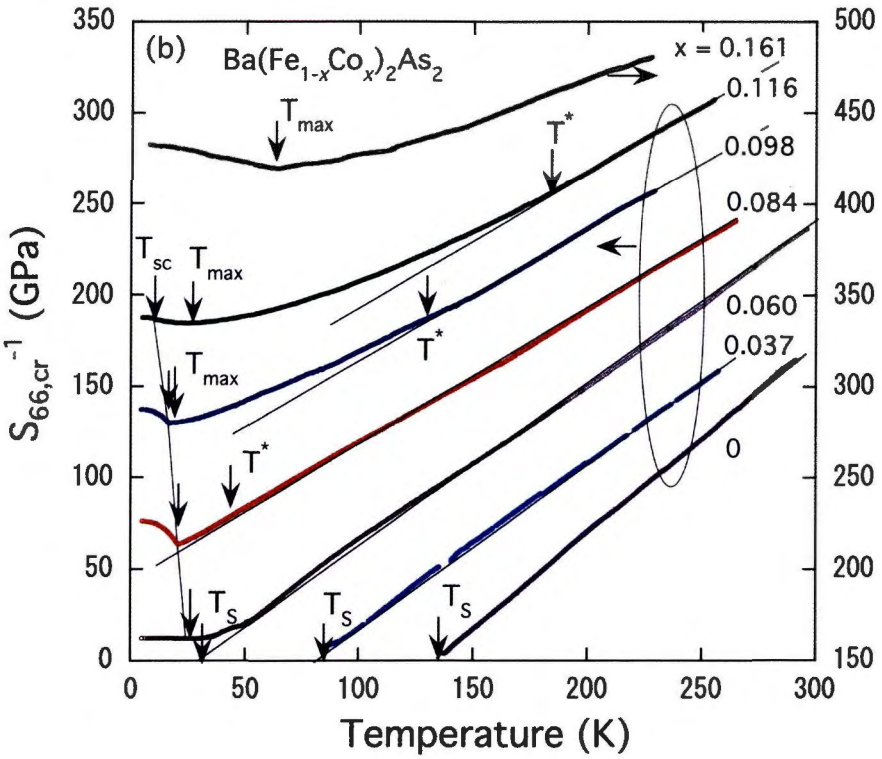

Figure 4.3: Temperature dependence of inverse of $S_{66,cr}$.

T_C in eq. 4.2 and T_S obtained from C_{66} are 134.3 and 141 K for $x = 0$, 81.4 and 84.7 K for $x = 0.037$, and 28.2 and 30.0K for $x = 0.060$, respectively. The magnetic transition at T_N could not observed in the C_{66} measurement owing to the disappearance of the echo signal below T_S. Our recent measurement of C_{33}, however, clearly shows the separation of $T_S = 84.7$ K and $T_N = 75.7$ K for $x = 0.037$. The closeness of T_S and T_C in each sample and the result on C_{33} for the 3.7% sample suggest that C_{66} softens toward T_S, and that the ferro-type crystal deformation

of ε_{XY} occurs below T_S.

4.1.2 Analysis based on band picture

The T dependence of C_{66} in the overdoped region can be explained by a band picture instead of by eq. 4.2. Large elastic anomalies compared with those of iron-based materials have been reported in the A15 superconductor V_3Si and the Laves-phase superconductor $CeRu_2$ so far [32, 33]. These anomalies have been ascribed to the large density of states at the Fermi energy. 3d orbitals form bands in an iron based superconductor. The bands located above the Fermi energy at the Γ-point form hole Fermi surfaces and electron pockets at M-points of the zone boundary[34]. In addition, the band nesting along the $[\frac{\pi}{a}, \frac{\pi}{a}, 0]$ direction is a key feature in iron-based superconductors. Here, we will consider the effects of bands. The bandwidth is affected by the crystal deformation, because the electron transfer (namely, transfer integral) between iron atoms would be modified by the lattice distortion. Therefore, equivalent four M-points in the tetragonal lattice do not become equivalent under the application of the strain ε_{XY}, as shown in Fig. 4.4. For example, the width of the bands at the Brillouin zone boundary M_1 and M_3 in Fig. 4.4 becomes large, and those of the bands at M_2 and M_4 become smaller under the application of ε_{XY}. This process gains the electronic energy, and looses the elastic energy. The amount of deformation is determined by the energy valance of the electronic and lattice energies. The formula

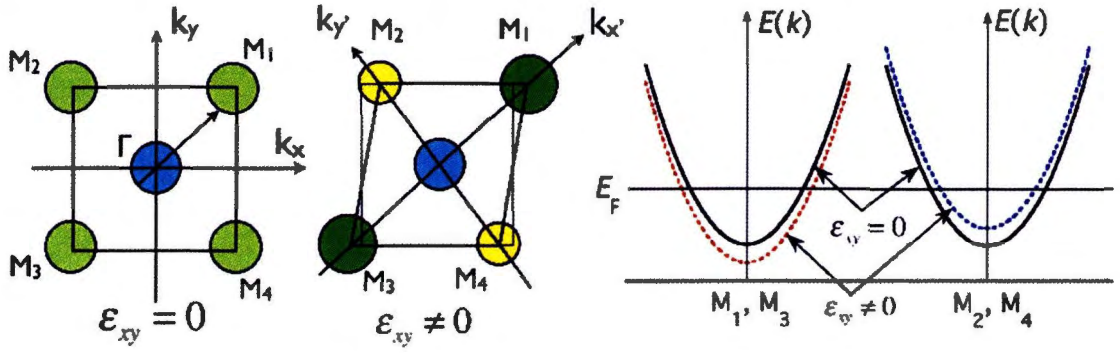

Figure 4.4: Effect of band on the crystal deformation. Four M points in square lattice do not become equivalent by the strain ε_{xy}, which makes the band consisting of d_{yz}/d_{zx} and $d_{x^2} - d_{y^2}$ degeneracy lifted..

for the elastic constant based on this consideration is as follows[35]:

$$
\begin{aligned}
C_{66} &= C_{66,0} - (d_{M1} - d_{M2})^2 \frac{\chi_S^0}{1 - I\chi_S^0} \\
\chi_S^0 &= \frac{1}{k_B T} \sum f_k(1 - f_k) \int dE N(E) f(E) \\
N(E) &= \frac{N_0}{2}[1 + (\frac{E - E_F}{W})^2]^{-1}
\end{aligned}
\tag{4.3}
$$

where f is the FermiDirac function, $d(= d_{M1} = d_{M2})$ is the electronlattice coupling constant, N_0 is the density of states at Fermi energy E_F, and I is the intersite interaction. The results of the fitting by adopting the Lorentzian density of states are shown in Fig. 4.5. In this analysis, the main adjustable parameter is the bandwidth W. We fixed $E_F/W = 0.4$ to obtain the best fitting. I is displayed in the figure, depending on x. We added a small constant ranging from 0.8 to 2.45 GPa to the experimental value of $C_{66,0}$ for the fitting. The W values were 100, 180, 250, and 450 K for the 8.4, 9.8, 11.6, and 16.1% samples, respectively. From the adjustable parameter $N_0 d^2$, d was respectively evaluated as

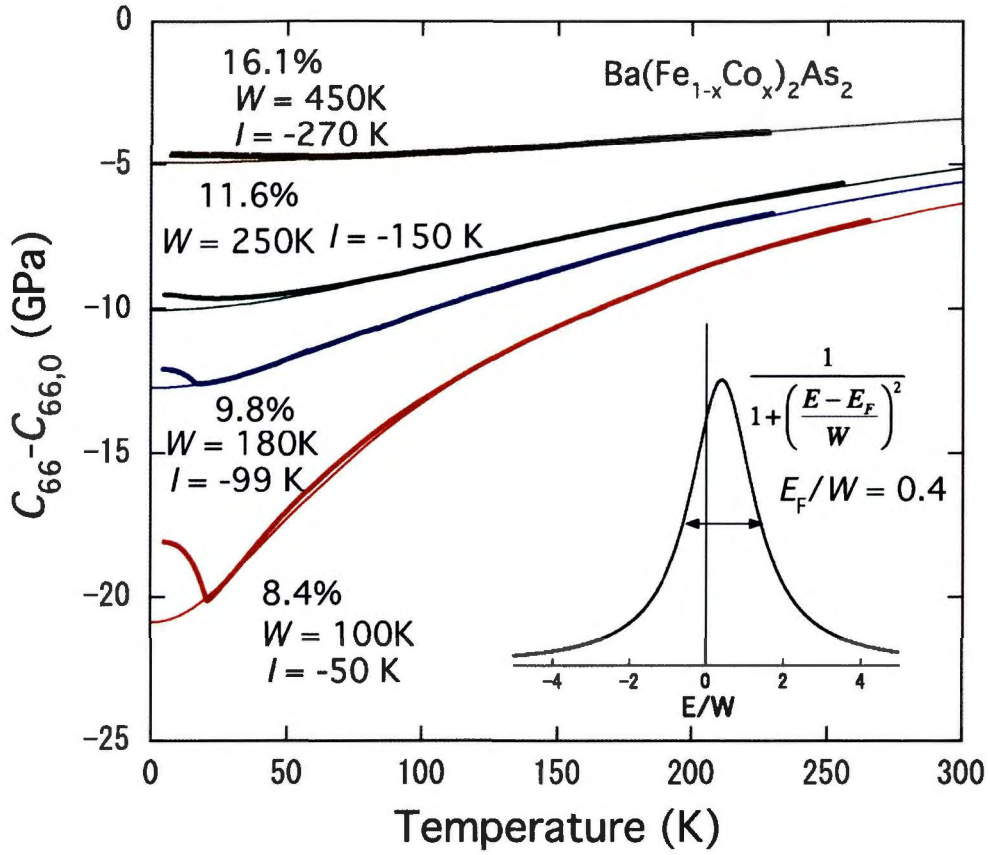

Figure 4.5: Theoretical fitting of C_{66} by the band JahnTeller effect under the assumption of Lorentzian density of states.

0.22, 0.25, 0.28, and 0.28 eV/Fe for the four samples, under the assumption that N_0 is approximately 1/W. The values of N_0 calculated from $N_0 = 1/W$ are respectively 110, 64, 46, and 26 states/eV for the four samples.

Note that eq. 3.14 is deduced to have the same form as eq. 4.1 for $T > W$. In this sense, eq. 3.14 includes eq. 4.2. However, eq. 3.14 is not applicable to analyzing the data of the underdoped samples, because W cannot be determined uniquely owing to the high T_S. Therefore, we consider that the adoption of the two types of analysis for the underdoped and overdoped samples is reasonable.

The band effect discussed here is called the electronic redistribution mechanism [36] and is applicable to systems having a low resistivity. It is supported experimentally. The resistivity of this system becomes lower in the overdoped region than in the underdoped region. Band nesting along the $[\frac{\pi}{a}, \frac{\pi}{a}, 0]$ direction is a characteristic feature of iron-based superconductors. We have no tool for analyzing elastic data on the basis of band nesting. However, we infer that it has a similar effect to that discussed above, and may cause C_{66} softening.

4.2 Quantum criticality

Figure 4.6 shows a summary of the phase diagram of $Ba(Fe_{1-x}Co_x)_2As_2$. The Co concentration dependences of T_S and T_{sc} are highly consistent with previous results[37]. We found two characteristic temperatures, i.e., T^* and T_{max}. A possible explanation for T^* is the crossover from the non-Fermi liquid region to the Fermi liquid region. The boundary from the non-Fermi T dependence to the Fermi liquid T^2 dependence observed in the resistivity measurements is not clear for $Ba(Fe_{1-x}Co_x)_2As_2$[38]. However, the behavior observed in $BaFe_2(As_{1-x}P_x)_2$ is similar to that observed in the present study including the x dependence of the crossover region[39].

We found T_{max}, which corresponds to the temperature at which $S_{66,cr}$ takes its maximum (at which $1/S_{66,cr}$ takes its minimum), as shown in Figs. 4.3 and 4.7. For highly correlated electron systems such as

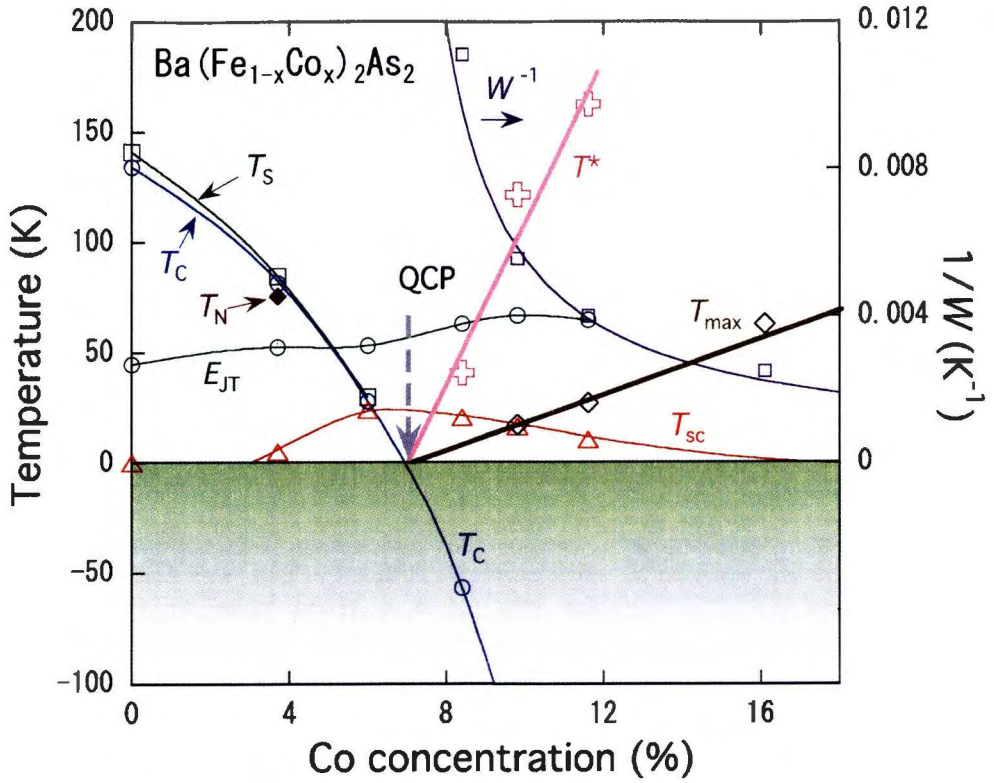

Figure 4.6: Phase diagram of $Ba(Fe_{1-x}Co_x)_2As_2$. The curves are visual guides.

$CeCu_2Si_2$, UPd_2Al_3, and UPt_3, a similar maximum was reported in the magnetic susceptibility χ and interpreted as a Kondo temperature, signaling the coherent motion of f-electrons[40]. From this analogy, T_{max} in this system suggests the onset of new coherent states.

Note that T^* and T_{max} approach zero at a QCP concentration of $x_C = 0.07$, indicating the existence of structural QCP at this concentration. In addition, the analysis based on the band picture suggests that the bandwidth W also approaches zero at the same x_C, which suggests a possible mass enhancement toward QCP in this system. Note that this point is located at the center of the superconducting dome. A similar phenomenon was reported for $BaFe_2(As_{1-x}P_x)_2$[41]. The obtained phase

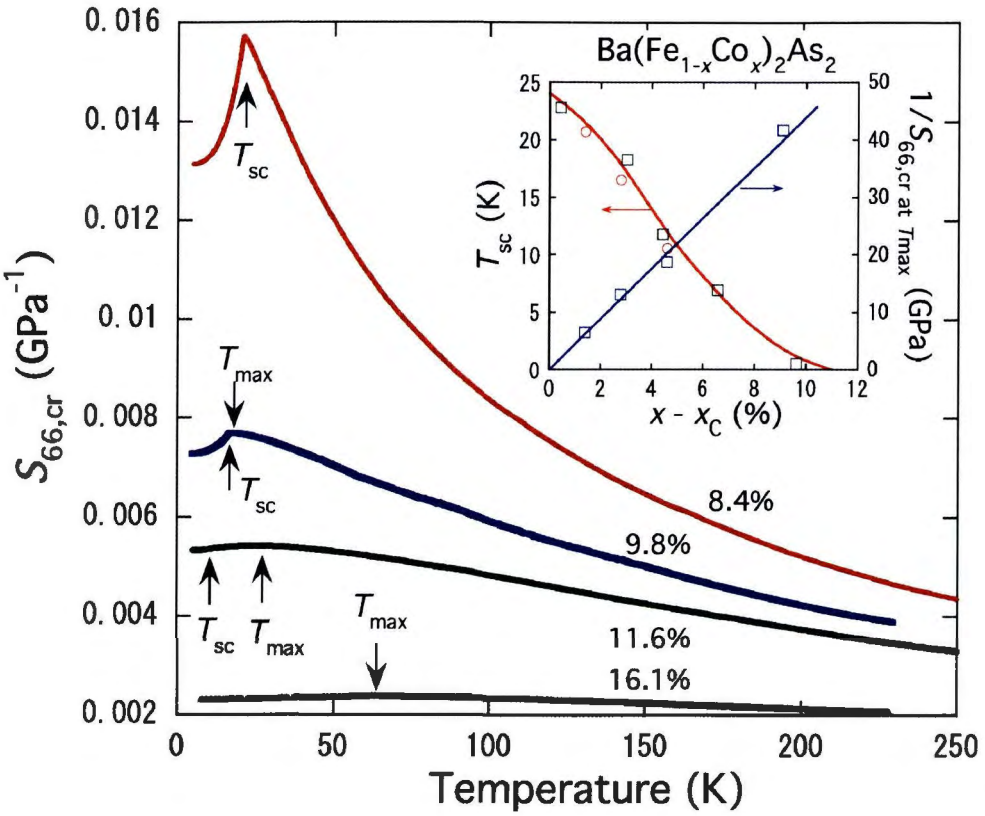

Figure 4.7: Temperature dependence of S66,cr for the overdoped samples. The inset shows the T_{sc} values from this work and ref. [37], and the inverse of the peak value of $S_{66,cr}$ as a function of the distance from the QCP concentration $x - x_C$. The curve of T_{sc} is a visual guide.

diagram and various phenomena near the QCP resemble those of well-known rare-earth compounds and uranium compounds. This coincidence strongly suggests the intimate relationship between superconductivity and QCP in this system, as in heavy fermion systems where magnetic QCP is presumed to be responsible for the emergence of unconventional superconductivity[42]. The essential difference in this case is that the quantum criticality is associated with structural fluctuations, unlike the magnetic fluctuations in previous cases. For this reason, we would like to call it the structural quantum criticality.

4.3 Correlation between elastic anomaly and superconductivity

We now discuss the relationship between elastic anomaly and superconductivity. As seen in the inset of Fig. 4.7, the amount of $1/S_{66,cr}$ is proportional to $x - x_C$, where x_C is the QCP concentration of Co; x_C= 0.07 for this system. Such a behavior is well known at the χ of the magnetic QCP. It is surprising that such a well-known behavior holds in this system with respect to S_{66} instead of χ for the magnetic system. As shown in the same figure, $T_{\rm sc}$ decreases with increasing $x - x_C$. Therefore, we can recognize an apparent correlation between $T_{\rm sc}$ and $1/S_{66,cr}$, such that $T_{\rm sc}$ is a function of $1/S_{66,cr}$. The explanation for this interesting fact is speculated to be as follows. As shown in Fig. 4.8, the underdoped sample exhibits a small anomaly at $T_{\rm sc}$, while a large upturn at $T_{\rm sc}$ is seen in the overdoped samples. Once the system enters the orthorhombic phase from the tetragonal phase, structural fluctuations are suppressed in the ordered phase. In the overdoped samples, however, structural fluctuations still survive even at $T_{\rm sc}$. The amount of anomaly at $T_{\rm sc}$ correlates with the peak height of $S_{66,cr}$, which is a measure of structural fluctuation. The large anomaly at $T_{\rm sc}$ for the overdoped samples suggests a strong coupling between structural fluctuation and superconductivity. These facts suggest that the origin of $S_{66,cr}$ is deeply related to the emergence of superconductivity.

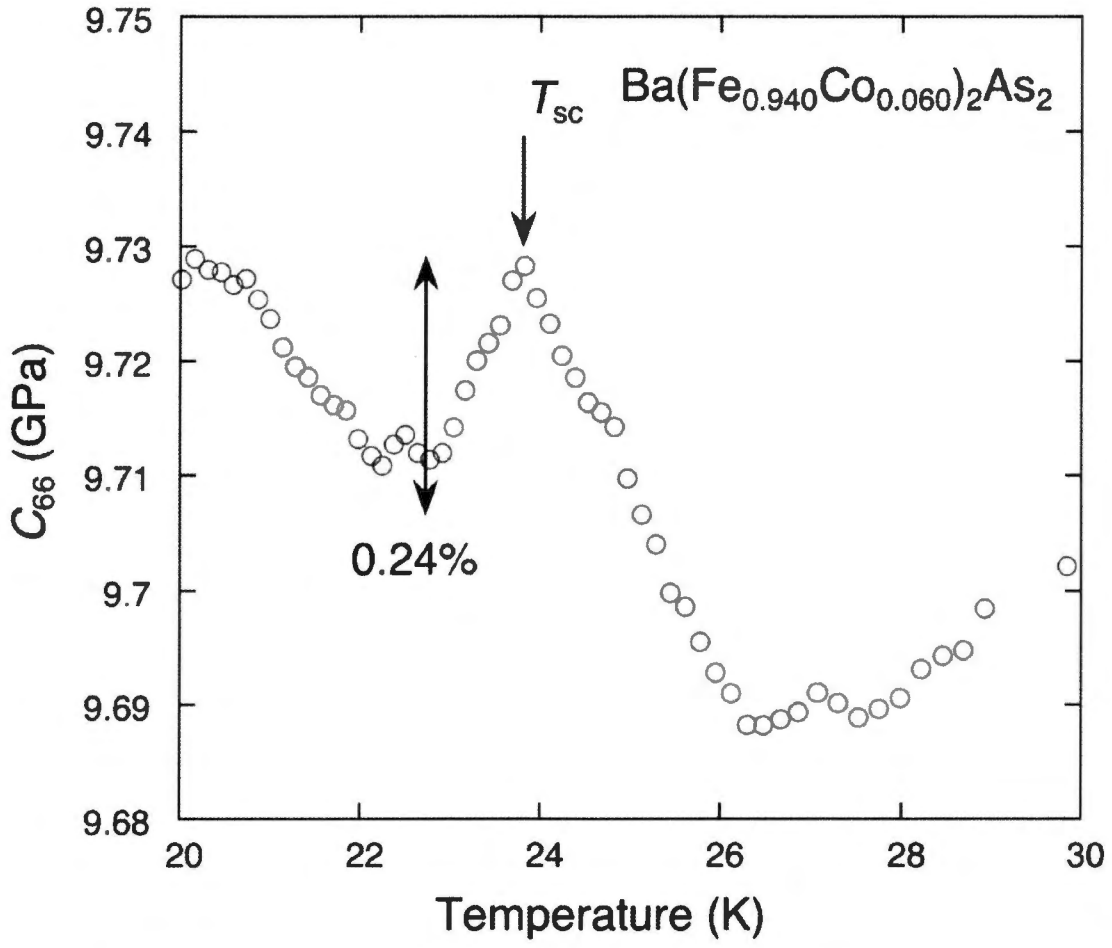

Figure 4.8: Temperature dependence of C_{66} for the overdoped $Ba(Fe_{0.940}Co_{0.060})_2As_2$ near T_{sc} in expanded scales.

Chapter 5

Strange inter-layer properties appearing in C_{33}

In this chapter we concentrate on our mind to the anomalous in C_{33}. As shown in Fig. 5.1 shows the temperature dependence of elastic constant C_{33} for all samples. One can see in the figure that, all samples show monotonic increase with decreasing temperature. The samples of x = 0, 0.037 show elastic softening at T_{N} and T_{S}. Overdoped samples of x = 0.084, 0.098, and 0.116 show a step-wise elastic anomaly at T_{sc}. Nearly optimal-doped sample of x = 0.060 shows remarkable elastic anomalies at T_{sc} and T_{N}. The appearance of elastic anomaly in C_{33} for under-doped, optimal doped, and over-doped samples would be reflected from a three-dimensional character of the iron-based superconductor $Ba(Fe_{1-x}Co_x)_2As_2$. Next, we will report peculiar physical properties of $Ba(Fe_{0.94}Co_{0.06})_2As_2$, which is located near to the QCP. For this Co concentration, we have studied the elastic properties, specific heat and electrical resistivity for two samples of different batch. A clear sam-

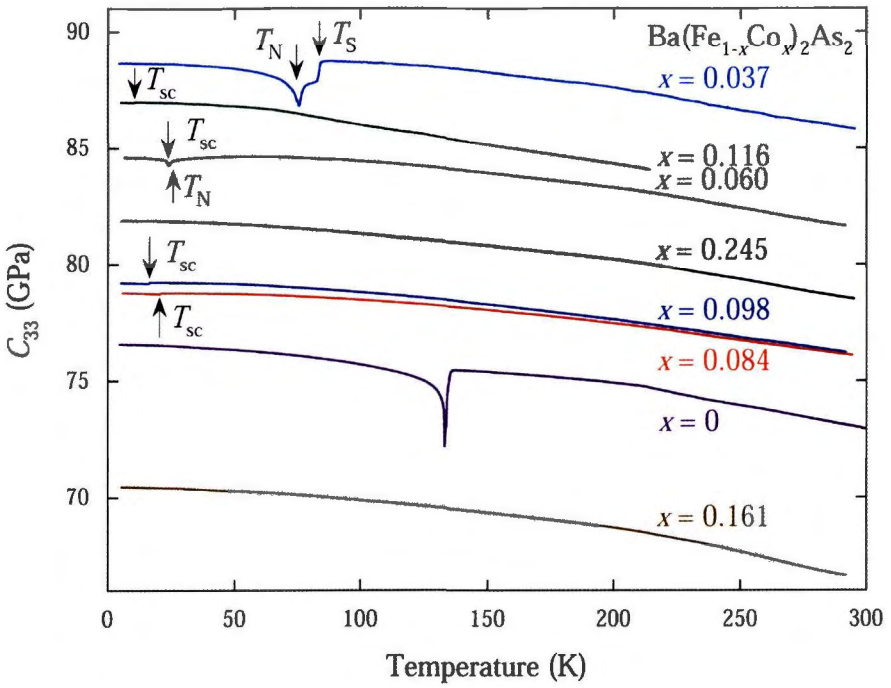

Figure 5.1: Temperature dependence of elastic constant C_{33} of $Ba(Fe_{1-x}Co_x)_2As_2$. Where x = 0, 0.037, 0.060, 0.084, 0.098, 0.116, 0.161, 0.245 respectively.

ple dependence for this composition was proved by careful inspection of elastic constants C_{33} and C_{66}, resistivity, and elastic attenuation α. According to the phase diagram of Ba122, the structural, magnetic, and superconducting phase transitions closely located to each other for 6% Co-doped sample. So to determine at which phases the elastic anomalous are occurred, we have carried out a simultaneous measurements of the electrical resistivity and elastic constant by one setting, where superconductivity is evident from a sharp drop to zero in the resistivity at 24 K for sample B, 24.2 K for sample D. These results of the electrical resistivity associated with the superconducting transition were also followed by the heat capacity measurement.

Figures 5.2(a) and (b) show temperature dependence of the elastic

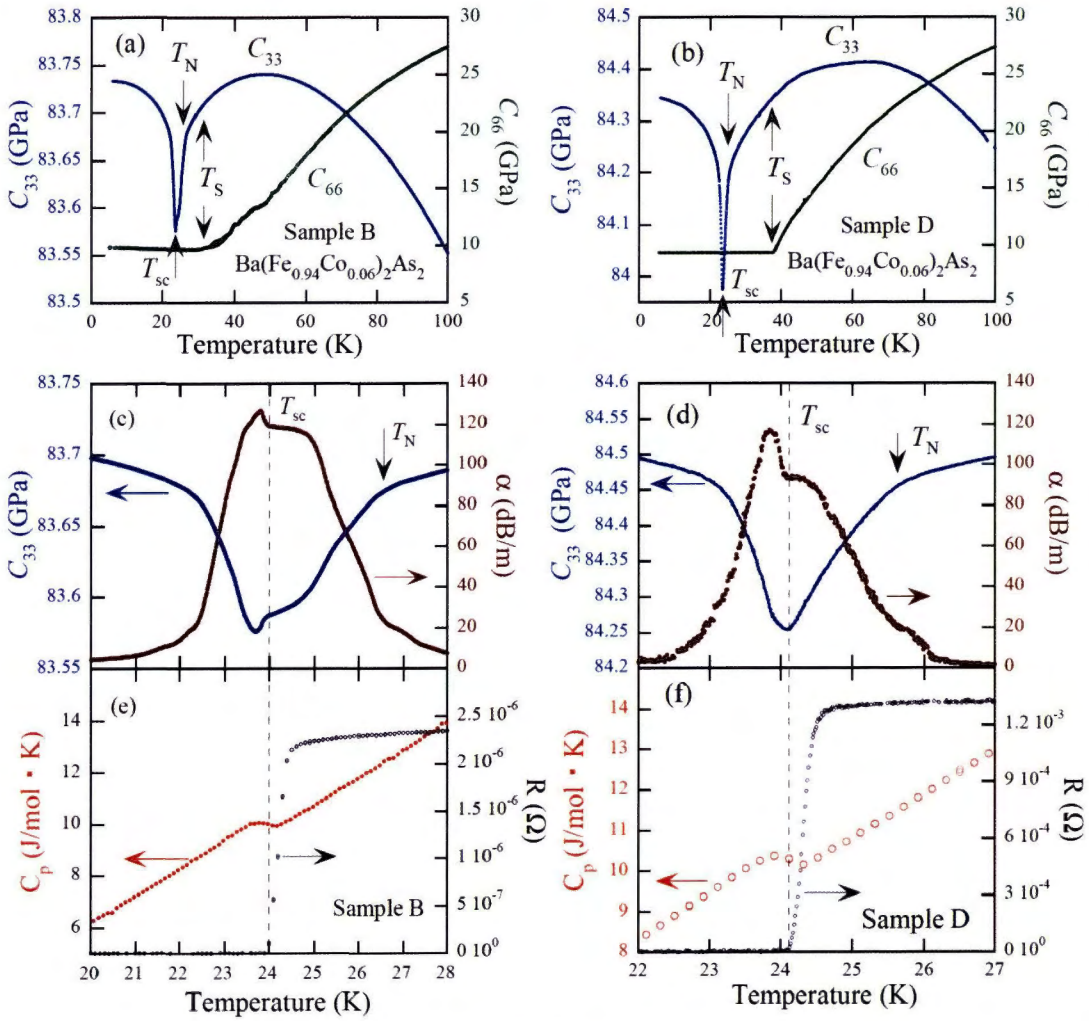

Figure 5.2: (Color online) (a) The temperature dependence of elastic constant C_{33} and C_{66} for optimal doped sample B. (b) Temperature dependence of elastic constant C_{33} and C_{66} for optimal doped sample D. (c) Temperature dependence of elastic constant C_{33} and attenuation of longitudinal elastic constant for optimal doped sample B. (d) Temperature dependence of elastic constant C_{33} and attenuation of longitudinal elastic constant for optimal doped sample D. (e) Temperature dependence of heat capacity and electrical resistivity near the superconducting phase transition temperature for optimal doped sample B. (f) Temperature dependence of heat capacity and electrical resistivity near the superconducting phase transition temperature for optimal doped sample D.

constants C_{33} and C_{66}. C_{66} shows large elastic softening from room temperature to low temperatures, and an inflection at T_S. In the case of C_{66}, both samples show elastic softening at T_S, but a small elastic anomaly was observed at T_{sc} and no anomaly at T_N. On the other hand, C_{33} shows a remarkable softening from 50 - 60 K towards T_N and T_{sc}. C_{33} drops steeply below a certain temperature above T_{sc}, which is considered to be T_N. C_{33} shows a minimum near T_{sc}, and increases rapidly with decreasing temperature. Precisely, sample B shows a step-wise anomaly at T_{sc}, while sample D shows no such anomaly near T_{sc}. It would be noted that both samples show no anomaly at T_S.

According to specific heat and resistivity in Figs. 5.2(e) and (f), specific heat anomaly was observed at T_{sc}, and no anomaly at T_N. The C_{33} in sample B and sample D show rather large softening towards T_N and/or T_{sc}. The amount of softening is 0.2% for sample B and 0.5% for sample D. For this analysis, it would be interesting what is the main factor for the softening in which, it starts from high temperature region such as 50 - 60 K. In general, it has been told that fluctuations associated with superconductivity does not start from such a high temperature, and appear just above T_{sc}. They cannot bring a large elastic softening. To the best of our knowledge, the largest elastic softening associated with superconductivity appears in organic superconductor κ-$(ET)_2X$ (X = $Cu(NCS)_2$, $Cu[N(CN)_2]Br$), which was found by Simizu.[45] Even in this case, the softening starts from $1.2T_{sc}$ at most. On the other hand the softening in C_{33} starts from almost $2T_{sc}$ for sample B and $3T_{sc}$ for

sample D, it implies that the elastic behavior in C_{33} is not from the superconducting origin. From our results, we would like to conclude that the anomaly in C_{33} is possibly ascribed to magnetic origin, although the origin still is an enigma.

We have also studied the ultrasonic attenuation α of the longitudinal elastic waves propagating along the c-axis for both samples. In Figs. 5.2(c) and (d), C_{33} and α are depicted as a function of temperature in an expanded scale. Although there are precise differences between sample B and D, we found interesting common features in C_{33} and α. The α shows a maximum at around $T_{\rm sc}$ and an additional peak below $T_{\rm sc}$ for both samples. Similar maximum in the ultrasonic attenuation was reported for $BaFe_{1.85}Ni_{0.15}As_2$ polycrystalline[46]. Usually, the ultrasonic attenuation decreases below $T_{\rm sc}$. Historically, some heavy electron superconductors UBe_{13} and UPt_3 showed an ultrasonic attenuation peak below $T_{\rm sc}$, which was discussed theoretically based on Landau-Khalatnikov damping mechanism[48, 47, 49]. It is associated with the relaxation of order parameter amplitude, which was found in superfluid He at first.[50] From the same point of view as Heavy fermion superconductor, the coupling between the superconducting gap amplitude and long wave length phonon was discussed for the case of a charge density-wave (CDW) compound $NbSe_2$.[51] The attenuation peak below $T_{\rm sc}$ for $Ba(Fe_{0.94}Co_{0.06})_2As_2$ would be caused by the same origin as the Heavy fermion superconductors and /or CDW compound, but the origin is still open.

For over doped samples, C_{33} shows a small but sharp softening towards T_{sc} results are shown in Fig. 5.3. In elastic constant measurements, there are two types of coupling between the order parameter M and elastic strain ε. One is bilinear coupling having the form of $M\varepsilon$, the other one is magneto-elastic coupling having the form of $M^2\varepsilon$. Bilinear coupling brings about large elastic softening from high temperature, which was seen in C_{66}. On the other hand, magneto-elastic coupling brings only a step-wise elastic anomaly. In general it does not show large anomaly compared to the bilinear coupling. In 6.0 % doped sample, the softening in C_{33} starts from high temperatures, which resembles that the large softening in C_{33} originated from the bilinear coupling. It would be possible origin for C_{33} anomaly, but it is an enigma. Important point is that there is no anomaly at T_S, but there is an anomaly at T_N. This fact suggests the importance of magneto-elastic coupling in C_{33} elastic anomaly. For over doped samples, C_{33} shows a small but sharp softening towards T_{sc}, so the elastic anomaly in C_{33} for $x = 0.060$, 0.084, 0.098, and 0.116 suggests that the coupling between the order parameter and elastic strain is $M^2\varepsilon$.

In Fig. 5.3, we plotted a relative amount of softening, which is normalized the data at 120 K as $\Delta C_{33}/C_{33}(x,T) = C_{33}(24.5\%,T)/C_{33}(x,T) - 1$. The normalized data $\Delta C_{33}/C_{33}$ merge at 120 K. Overdoped samples show remarkable step-wise anomaly at T_{sc}. Unlike 6.0 % doped sample, obove the T_{sc} in overall temperature range, overdoped samples show monotonic increase with decreasing temperature. However when

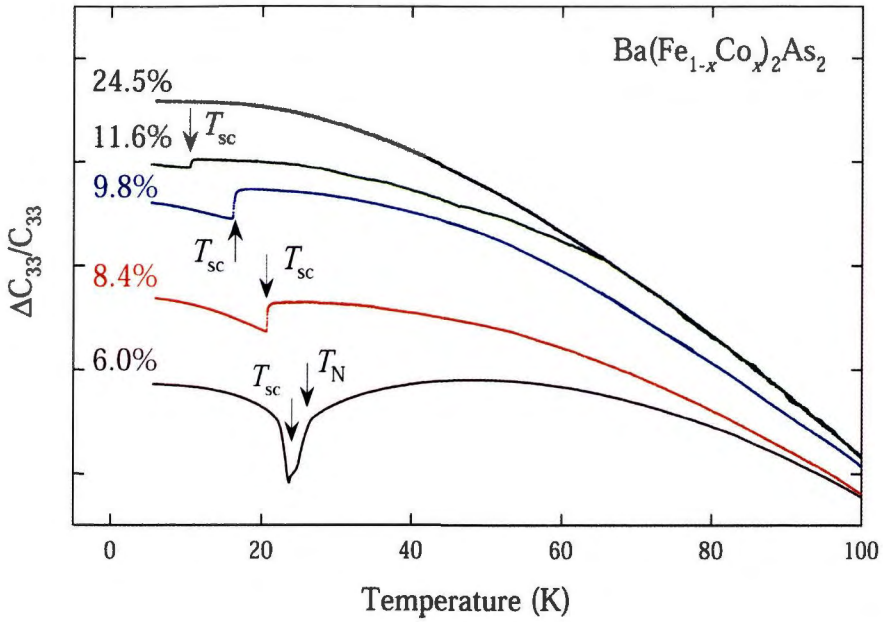

Figure 5.3: Temperature dependence of elastic constant C_{33} of overdoped samples.

we regard 24.5 % sample as the back ground, overdoped samples show anomaly towards low temperatures same as 6.0 % doped sample. The amount of softening is defined by $\Delta C_{33}/C_{33} = \Delta C_{33}(24.5\%, T_{\rm sc})/C_{33}(24.5\%, 120K) - \Delta C_{33}(x, T_{sc}(x))/C_{33}(x, 120K)$.

This amount becomes larger as approaching to the QCP.

Second, we will discuss about Grüneisen parameter. Grüneisen constant is a scale of magnitude and order parameter so called the interaction of order parameter and distortion of the magneto-strictive coupling. Grüneisen parameter $\Omega_{\rm sc}$ for $T_{\rm sc}$ can be defined by the relation:

$$\Omega_{\rm sc} = \frac{C_\Gamma}{T_{\rm sc}} \frac{\partial T_{\rm sc}}{\partial P} \tag{5.1}$$

$$\Omega = -\frac{1}{T_{sc}} \left(\frac{\partial T_{sc}}{\partial \varepsilon} \right) \tag{5.2}$$

where $T_{\rm sc}$ is the superconducting phase transition temperature, C_{Γ} is the bulk modules.

Firstly, lets define the derivation of the uniaxial-pressure function of $\frac{\partial T_{sc}}{\partial p}$. The Ehrenfest relationship in thermodynamics is established at the time of second order phase transition. Following equation holds change does not occur in entropy before and after the transition to the secondary phase transition.

$$S_1(T_{\rm sc}, p) = S_2(T_{\rm sc}, p) \tag{5.3}$$

make a full differential for both sides, it will be change,

$$\left(\frac{\partial S_1}{\partial T_{sc}}\right)_p dT_{sc} + \left(\frac{\partial S_1}{\partial p}\right)_{T_{sc}} dp = \left(\frac{\partial S_2}{\partial T_{sc}}\right)_p dT_{sc} + \left(\frac{\partial S_2}{\partial p}\right)_{T_{\rm sc}} dp \tag{5.4}$$

here,

$$C_p = T_{\rm sc}\left(\frac{\partial S}{\partial T_{\rm sc}}\right)_p, \quad \left(\frac{\partial S}{\partial T_{sc}}\right)_p = \frac{C_p}{T_{\rm sc}} \tag{5.5}$$

$$\begin{aligned} S = -\left(\frac{\partial G}{\partial T}\right), \quad V &= \left(\frac{\partial G}{\partial p}\right)_T \left(\frac{\partial S}{\partial p}\right)_T = -\frac{\partial}{\partial p}\left(\frac{\partial G}{\partial T}\right)_p \\ &= -\frac{\partial}{\partial T}\left(\frac{\partial G}{\partial p}\right)_T = -\left(\frac{\partial V}{\partial T}\right)_p \end{aligned} \tag{5.6}$$

then

$$\left\{\left(\frac{\partial S_1}{\partial T_{\rm sc}}\right)_p - \left(\frac{\partial S_2}{\partial T_{\rm sc}}\right)_p\right\} dT_{\rm sc} = \left\{-\left(\frac{\partial S_1}{\partial p}\right)_T + \left(\frac{\partial S_2}{\partial p}\right)_T dp\right\} \tag{5.7}$$

$$\frac{1}{T_{sc}}\left(C_{p1} - C_{p2}\right) dT_{\rm sc} = \left\{\left(\frac{\partial V_{m1}}{\partial T_{\rm sc}}\right)_p - \left(\frac{\partial V_{m2}}{\partial T_{\rm sc}}\right)_p\right\} dp \tag{5.8}$$

$$\frac{\partial T_{\rm sc}}{\partial p} = \frac{1}{V}\frac{\Delta\beta}{\Delta C_p/T_{\rm sc}} \tag{5.9}$$

where $\Delta\beta$ is the volume expansion, if we replace the volume expansion by the linear expansion coefficient $\Delta\alpha$, uniaxial-pressure dependence of $T_{\rm sc}$ becomes

$$\frac{\partial T_{\rm sc}}{dp_{\rm i}} = \frac{1}{V}\frac{\Delta\alpha_i}{\Delta C_{\rm p}/T_{\rm sc}} \tag{5.10}$$

then the Grüneisen constant takes the definition of

$$\Omega_i = \frac{C_\Gamma}{T_{\rm sc}}\frac{\partial T_{\rm sc}}{\partial p_{\rm i}} \tag{5.11}$$

on the other hand, the elastic constant from the second derivative by the distortion of the free energy F

$$F = Tf(T - T_{\rm sc}) \tag{5.12}$$

if this form differentiated by the strain ε, then it becomes

$$\frac{\partial F}{\partial \varepsilon} = \frac{\partial}{\partial \varepsilon}\left\{Tf(T - T_{\rm sc})\right\} = -T\frac{\partial f(T - T_{sc})}{\partial(T - T_{sc})} \cdot \frac{\partial T_{sc}}{\partial \varepsilon} \quad . \tag{5.13}$$

by further differentiating

$$C_\Gamma = \frac{\partial^2 F}{\partial \varepsilon^2} = \frac{\partial}{\partial \varepsilon}\left\{ -T\frac{\partial f(T-T_{sc})}{\partial (T-T_{\rm sc})} \cdot \frac{\partial T_{\rm sc}}{\partial \varepsilon} \right\} = T\frac{\partial^2 f(T-T_{\rm sc})}{\partial (T-T_{\rm sc})^2}\left(\frac{T_{\rm sc}}{\partial \varepsilon}\right)^2 \tag{5.14}$$

in addition, entropy S and internal energy U is become

$$U = F + TS, \quad S = -\left(\frac{\partial F}{\partial T}\right)_V \tag{5.15}$$

so, we can write it

$$U = F - T\left(\frac{\partial F}{\partial T}\right)_v = -T^2\left\{\frac{(F/T)}{\partial T}\right\}_v \tag{5.16}$$

therefore, the specific heat C_V is,

$$C_V = \frac{\partial U}{\partial T} = -\frac{\partial}{\partial T}\left[T_{\rm sc}^2\left\{\frac{\partial (F/T)}{\partial (T-T_{\rm sc})}\right\}_V\right] = -2T_{\rm sc}\frac{\partial (F/T)}{\partial (T-T_{\rm sc})} - T^2\frac{\partial (F/T)}{\partial (T-T_{\rm sc})^2} \tag{5.17}$$

here, considering only the second term we can get

$$\frac{\partial^2 f(T-T_{\rm sc})}{\partial (T-T_{\rm sc})} = -\frac{\Delta C_V}{T_{\rm sc}^2} \tag{5.18}$$

if we input this formula in to 5.14 then,

$$\Delta C_\Gamma = -\frac{T_{\rm sc}}{T^2} \cdot \Delta C_{\rm V}\left(\frac{\partial T_{\rm sc}}{\partial \varepsilon}\right)^2 \tag{5.19}$$

the definition of Grüneisen constant Ω from 5.2

$$\begin{aligned} \Delta C_\Gamma &= -T_{\rm sc}\Delta C_V \Omega^2 \\ \Omega^2 &= \left| \frac{\Delta C_\Gamma}{\Delta C_V T_{\rm sc}} \right| \end{aligned} \tag{5.20}$$

In this research we ha calculated the The Grüneisen constant from the jump in specific heat and the jump in elastic moduli at $T_{\rm sc}$ by

$$\Delta C = -\Omega_{\rm sc}^2 \Delta C_{\rm v} T_{\rm sc}. \tag{5.21}$$

The jump at the superconducting phase transition temperature of C_{33} and the heat capacity were pictured in Fig. 5.4 for under doped region, and in Fig. 5.5 for over doped region. The jumps in C_{11} for overdoped samples at $T_{\rm sc}$ was pictured in Fig. 5.5.

Grüneisen parameter has a small value near the QCP, and gradually increases with the increasing of Co concentration in over-doped region. Our estimation can be checked by the previous works. The Grüneisen parameter defined by

$$\Omega_{\rm sc} = -\frac{1}{T_{\rm sc}} \frac{dT_{\rm sc}}{d\varepsilon_{\rm i}}. \tag{5.22}$$

Here the uniaxial strain dependence $dT_{\rm sc}/d\varepsilon_{\rm i}$ is related to uniaxial pressure dependence of $T_{\rm sc}$ as

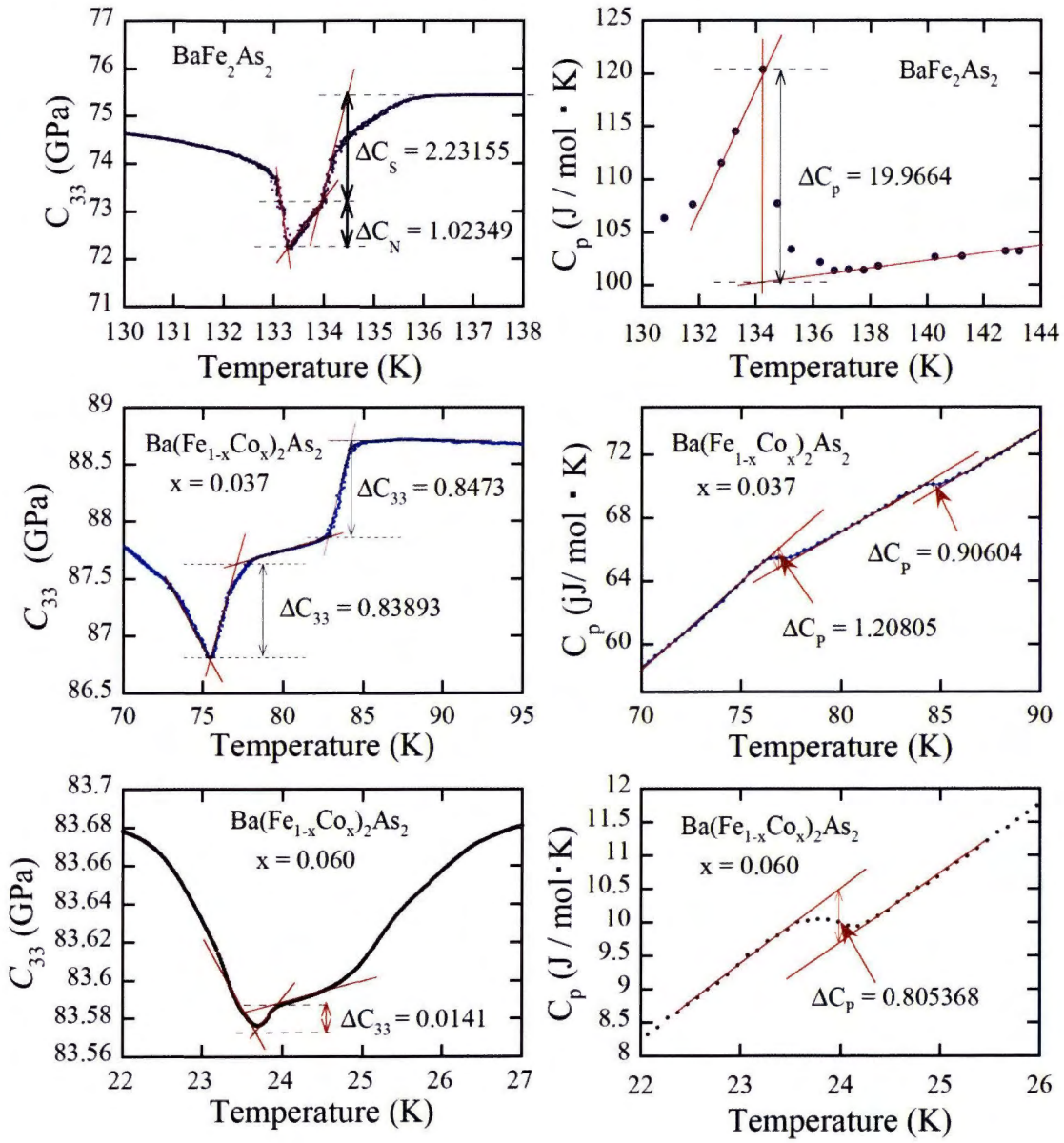

Figure 5.4: Jumps near the phase transitions in elastic constant C_{33}(on the left) and specific heat(on the right).

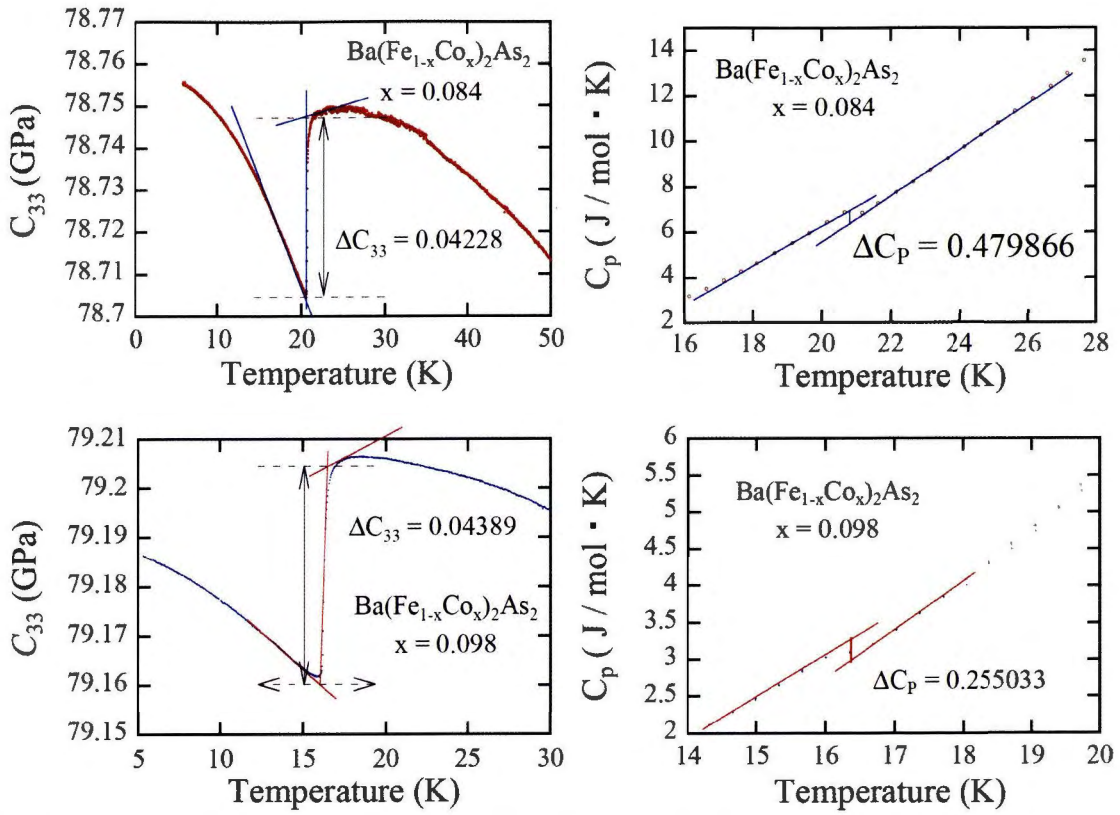

Figure 5.5: Jumps near the phase transitions in elastic constant C_{33}(on the left) and specific heat(on the right).

$$\frac{dT_{\rm sc}}{d\varepsilon_{\rm xx}} = -C_{11}\frac{dT_{\rm sc}}{dp_{\rm a}} - C_{12}\frac{dT_{\rm sc}}{dp_{\rm a}} - C_{13}\frac{dT_{\rm sc}}{dp_{\rm c}} \tag{5.23}$$

$$\frac{dT_{\rm sc}}{d\varepsilon_{\rm zz}} = -C_{33}\frac{dT_{\rm sc}}{dp_{\rm c}} - 2C_{13}\frac{dT_{\rm sc}}{dp_{\rm a}} \tag{5.24}$$

where i is 1 for XX and a-axis, and 3 for ZZ and c-axis. $C_{\rm ij}$ is the corresponding elastic constants, and $dT_{\rm sc}/dp_{\rm i}$ is the uniaxial pressure dependencies of $T_{\rm sc}$. We can calculate Ω from the elastic constant and uniaxial pressure dependence of $T_{\rm sc}$.

We would like to compare our results with the previous works. Bud'ko

et al. reported these values of dT_{sc}/dp_i for 3.8 % and 7.4 %, and Hardy et al. reported it for 8.0 %. Bud'ko et al. obtained $dT_{sc}/dp_a = -4.1$ K/kbar and $dT_{sc}/dp_c = 1.7$ K/kbar for 3.8%, $dT_{sc}/dp_a = 0.3$ K/kbar and $dT_{sc}/dp_c = -2.6$ K/kbar for 7.4% [29]. Hardy et al. obtained $dT_{sc}/dp_a = 3.1(1)$ K/GPa and $dT_{sc}/dp_c = -7.0(2)$ K/GPa for 8% [30] from thermal expansion measurement. We used these values of C_{11}, C_{33} and C_{12} to be 109.2 GPa, 78.7 GPa and 43.46 GPa, respectively, for the calculation. Since C_{13} cannot be obtained by our measurements, we assumed it to be the same value as C_{12}. In the case of 8% doped sample, Grüneisen constant and $dT_{sc}/d\varepsilon_{ZZ}$ are evaluated to be 14.2 and 282 K, respectively. The value of Ω is consistent with our result. On the other hand the predicted values did not achieved for 3.8% and 7.4%, it is ten times larger then our value. In the case of 3.8%, the calculated values are 716 K for $dT_{sc}/d\varepsilon_{ZZ}$ and 102.3 for Grüneisen constant, and 2037 K and 97 for 7.4%. They are inconsistent with our results and Hardy et al. The reason of the differences is an enigma. Here, we have to attention to the sign of the Grüneisen parameter. We cannot obtain the information about whether Ω is positive or negative, when it is evaluated from 5.21. On the other hand, 5.22 - 5.24 give its sign. dT_{sc}/dp_c is positive for underdoped samples, and negative for overdoped region. dT_{sc}/dp_a has an opposite sign of dT_{sc}/dp_c. Since the 6.0 % sample is located in the underdoped region, the sign of Ω might be negative. In addition, as long as hydrostatic pressure concern the changing of T_{sc} is positive for underdoped samples, and negative for overdoped samples. This behavior

Table 5.1: Estimated values of T_{sc}, ΔC_{33}, and $\Delta C_p/T_{sc}$ and calculated strain dependence of $dT_{\rm sc}/dp_c$, $dT_{\rm sc}/d\varepsilon_{zz}$, and Ω for 6%, 8.4%, and 9.8%.

x-Co(%)	0.06	0.084	0.098
T_{sc} (K)	24	16.7	20.6
ΔC_{11} (10^{-2}GPa)	1.5	2.5	1.96
ΔC_{33} (10^{-2}GPa)	1.4	4.2	4.4
$\Delta C_p/T_{sc}$ (mJ/mol·K^2)	33	23	15
$dT_{\rm sc}/dp_a$ K/GPa	1.84	2.32	2.49
$dT_{\rm sc}/dp_c$ K/GPa	1.9	4.2	5.3
$dT_{\rm sc}/d\varepsilon_{xx}$	163	258	280
$dT_{\rm sc}/d\varepsilon_{zz}$	160	334	420
$\mid \Omega \mid_{33}$	6.7	16.2	25.2
$\mid \Omega \mid_{11}$	6.8	12.5	16.8

is similar to c-axis uniaxial pressure dependence of this system.[?] This implies that hydrostatic pressure dependence is due to the c-axis.

The calculated results of both $dT_{\rm sc}/d\varepsilon_{\rm a}$ and $dT_{\rm sc}/d\varepsilon_{\rm c}$ as a function of Co-concentration dependence re-listed in Table I for the overdoped samples.

Chapter 6

Large elastic softening in heavy fermion superconductor $Rh_{17}S_{15}$

6.0.1 Introduction

$Rh_{17}S_{15}$ mainly found near the Miass river in south part of Ural mountains in Russia. This compound firstly found by Matthias in 1954. Until now many minerals were found in this area. $Rh_{17}S_{15}$ belongs to the cubic space group $Pm3m$ with a lattice constant of 0.99093(2) nm. As shown in Fig. 6.1a (a), it contains a cage in the center of the structure. Otherwise the structure contains 2 f.u. with 64 atoms in the unit cell. As pictured in Fig. 6.1b (b), it contains four rhodium sites (1b, 3d, 6e and 24m), and three sulfur sites (12i, 12j and 6f)]. One of the important features of this structure is that the Rh(3d) has two Rh(6e) neighbors at 0.258 nm which is shorter than the nearest neighbor Rh-Rh distance (0.269 nm) in a cubic Rh metal. As shown in Fig. 6.1, it shows a superconducting at 5.4 K, and exhibiting shoulder like behavior around 100

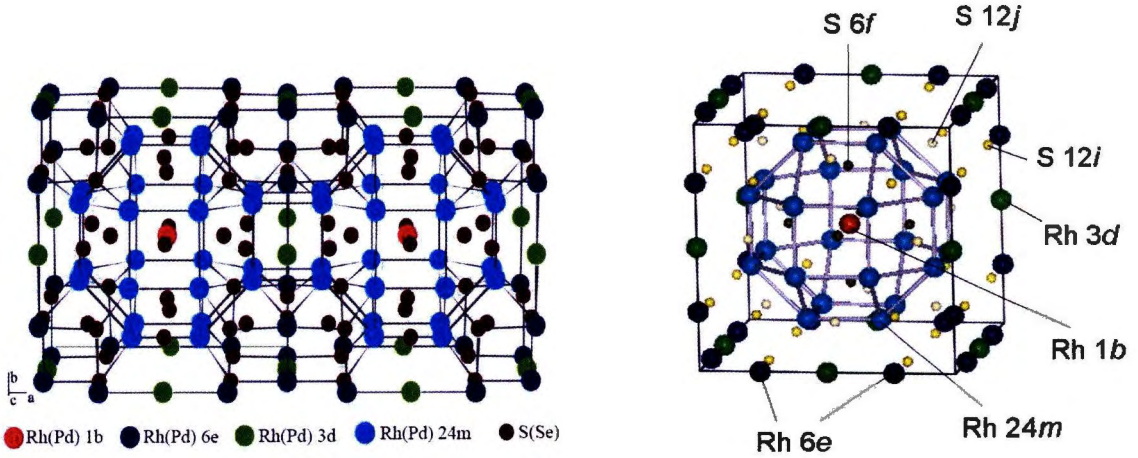

(a) (b)

Figure 6.1: (a) The crystal structure of $Rh_{17}S_{15}$ which consists of two formula units with 64 atoms in the unit cell. (b) $Rh_{17}S_{15}$ has 4 types of Rhodium atoms with position symmetry 24m, 6e, 3d and 1 b, and three sulfur sides (12i, 12j, 6f). Rh(d) has two shorter Rh(e) neighbors at 0.258 nm

K. Apart from this $Rh_{17}S_{15}$ has several interesting properties such as the temperature dependence of upper critical field estimates H_{c2} at $T =$ 0 K to be 23.5 T, which significantly exceeds the Pauli limit (9.99 T). The result of temperature dependence of the heat capacity indicates the strongly-coupled superconductivity by the fact that $\Delta C_{\rm p}/\gamma T_{\rm sc}$ is approximately 2.6 and this value is larger than 1.43 (BCS theoretical value). Moreover, normal state properties are worth mentioning as well. Sommerfeld constant takes a relatively large value (γ =110 mJ/mol K^2), and H. R. Naren *et al.* estimated the enhanced density of stated $N^*(0) = 46$ states/eV-formula unit, these above mentioned results were illustrated in Fig. 6.2, and 6.3.

The band structure of the $Rh_{17}S_{15}$ with the Density of States plot as shown in Fig. 6.4, one can imagine that both electron-like and hole-like pockets at the Fermi Level supporting the fact that there are both types

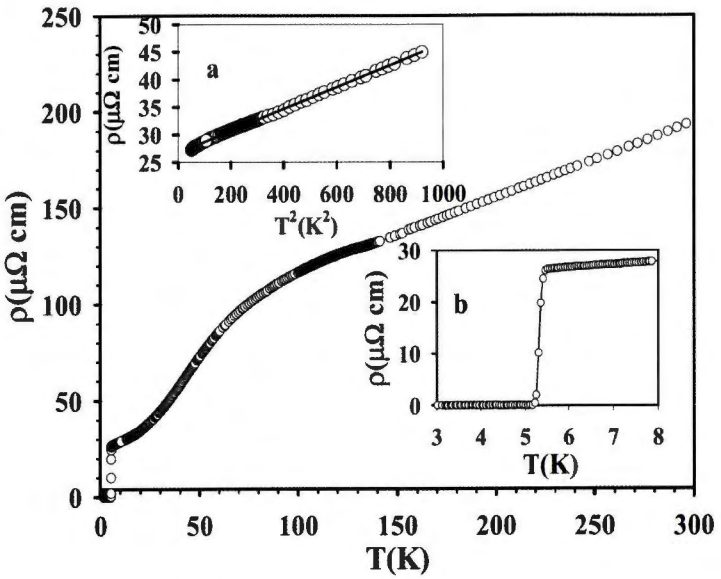

Figure 6.2: Temperature dependence of resistivity of the single crystal $Rh_{17}S_{15}$. Figure from. [54]

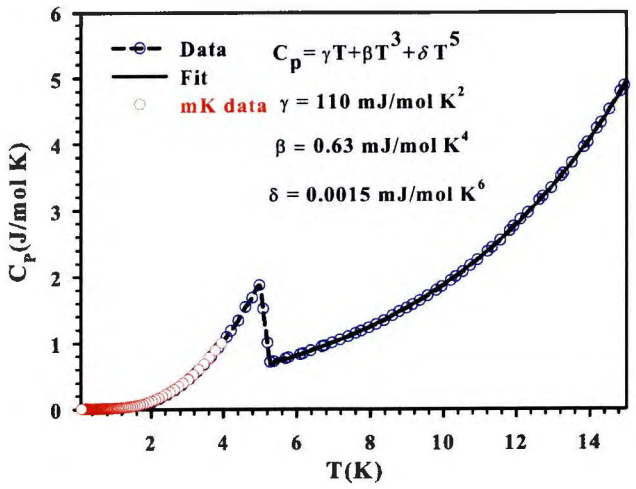

Figure 6.3: Temperature dependence of heat capacity of the single crystal $Rh_{17}S_{15}$. Figure from. [54]

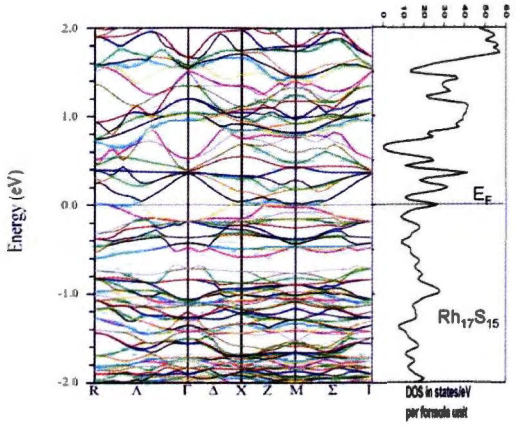

Figure 6.4: The band structure of $Rh_{17}S_{15}$. The total DOS is indicated on the right side of the plot. From [55].

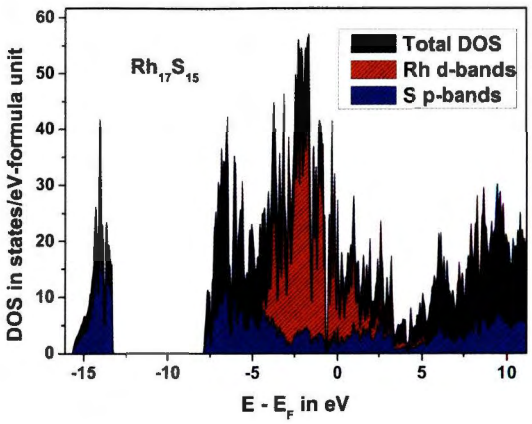

Figure 6.5: DOS for $Rh_{17}S_{15}$ from LDA (Local Density Approximation) calculations. Contributions of Rh and S are indicated in red and blue respectively. From [55].

of charge carriers in the system.

As shown in Fig. 6.5 the DOS plot in the total energy range of calculation indicates the large density of states at the Fermi level and estimate the electron-phonon coupling (λ) by

$$\lambda = \left(\frac{\text{DOS from heat capacity}}{\text{DOS from band structure}} \right) - 1 \qquad (6.1)$$

which gives a λ of 0.7.

The basic properties such as Sommerfeld coefficient, enhanced susceptibility and large upper critical field, in $Rh_{17}S_{15}$ [55] suggests a strong Rh-Rh interactions which form a large density of states at the Fermi level. As we know the 3d orbitals form the bands in an iron-based superconductors. Our group has reported a large elastic anomaly in C_{66} for $Ba(Fe_{1-x}Co_x)_2As_2$ [56], analyzed this elastic anomaly by band picture. Large elastic anomalies compared with those of iron-based materials have

been reported in the A15 superconductor V_3Si and the Laves-phase superconductor $CeRu_2$. In these compounds the anomalies have been ascribed to the large density of states at the Fermi level. So it is motivated us to study the elastic properties of this sample.

6.0.2 Sample for the Ultrasonic measurement

Figure 6.6: The picture of $Rh_{17}S_{15}$ (upper), and pulse echo of this sample (down).

In this research we have studied the longitudinal elastic constants C_{11}, C_L (C_L =1/2 (C_{11}+C_{12}+2C_{44})), and transverse elastic constants C_{44} and C_E =1/2(C_{11}-C_{12}). Sample was provided by Ōnuki, and Settai from Osaka University. The sample which was used in the ultrasonic measurement (the upper picture) and its echo shape (down picture) is seen in Fig. 6.6. The echo shape seen in the picture was obtained after polishing this sample. The tools for polish were pictured in Fig. 6.6. We used PHTHALICGLUE to stabilize the sample on the polish set.

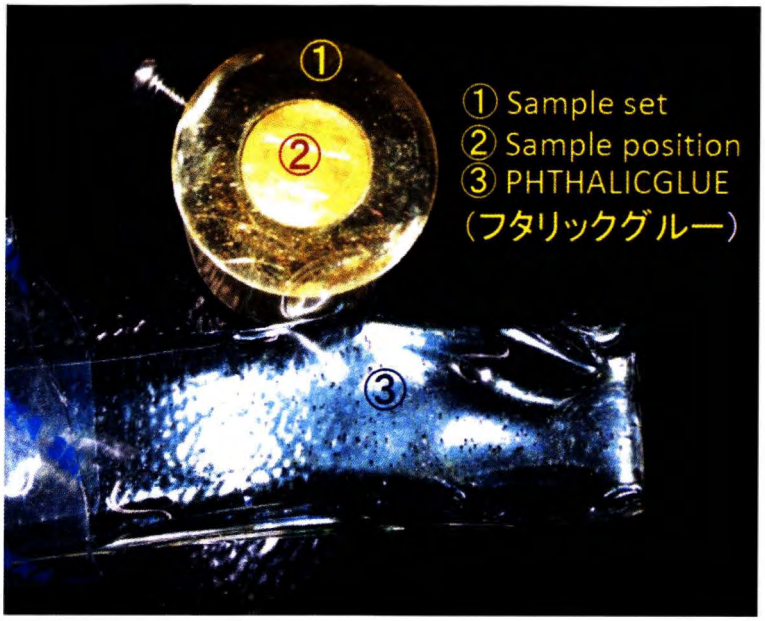

Figure 6.7: Tools for the polish.

6.1 Experimental results and discussions

$Rh_{17}S_{15}$ has the cubic crystal symmetry, then it has three elastic constants C_{11}, C_{44}, and C_{12}. We have measured all elastic constants for this sample. As you can see in Fig. 6.7 all elastic constants show monotonic increase with decreasing temperature above certain temperatures and then turn to decrease until superconducting phase transition temperature. The amount of softening is 6.63 %, 0.61 %, 1.66 %, and 17.5 % for C_{11}, C_{44}, C_{L}, and C_{E} respectively. All elastic constants show an anomaly at 5.4 K it corresponds to the superconducting phase transition. Among them the C_{E} (C_{E} equals to $1/2(C_{11} - C_{12})$) shows large elastic softening of 17.5 %.

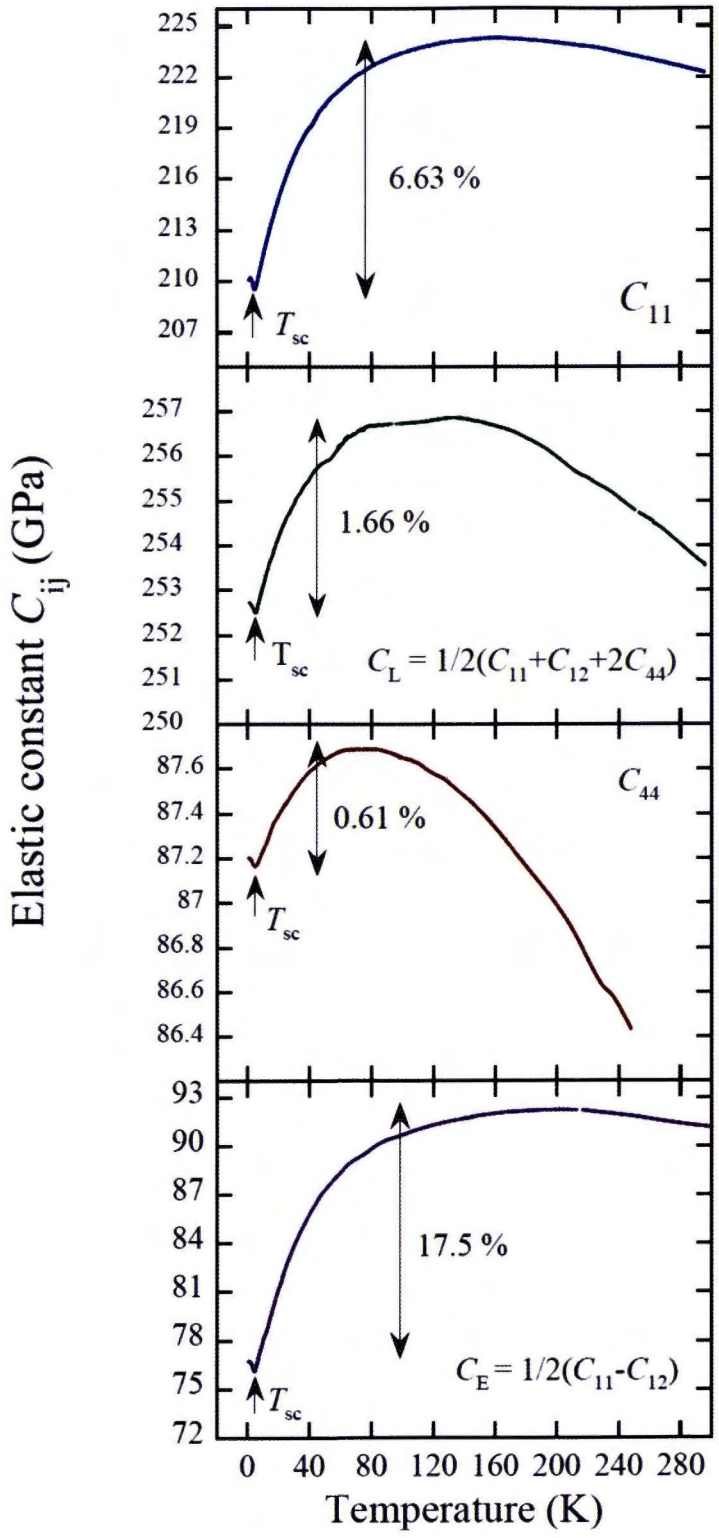

Figure 6.8: Temperature dependence of elastic constant of the single crystal $Rh_{17}S_{15}$.

6.1.1 Magnetic field dependence of C_{E}

We have also studied the magnetic field dependence of elastic constant C_{E} of this sample. When we increase the magnetic field the elastic anomaly at T_{sc} becomes small and shifts to low temperature side as pictured in Fig. 6.9. Decreasing of T_{sc} with the increasing of magnetic field is corresponds to the magnetic field dependence of the resistivity of this sample which was measured by R. Settai *et al.* [57].

6.1.2 Effect of band to the large elastic softening in C_{E}

Deformations of the lattice caused by sound waves or phonons modify the charge distribution and lattice potential which leads to a coupling between conduction electrons and phonon. It causes a temperature dependence of elastic constants. According to the band calculations the bands located above the Fermi energy at the γ point form electron pockets at M-points of the zone boundary. We believe that if a large density of states exists at the M-point, an elastic anomaly may be caused. Fig. ?? is an illustration for the effect of band on the crystal deformation under the γ_3 symmetry strain $\varepsilon_{xx} - \varepsilon_{yy}$. By the application of $\varepsilon_{xx} - \varepsilon_{yy}$, the bands at two locations X_x are pushed up and the others (X_y) are pulled down. Maybe this illustration provides why the large elastic anomaly occurs in the elastic constant C_{E}. A rigid two band model with constant density of states N_A, and N_B gives

$$C_{\Gamma} = C_{\Gamma}^{0} - (\langle d_A \rangle - \langle d_B \rangle)^2 N_A f_A f_B / [N_A f_A + N_B f_B] \qquad (6.2)$$

and for the special case

$N_{A,B} = N_0, \langle d_A \rangle = -\langle d_B \rangle = d$ and $n = 2N_0(E_F - E_0)$

one obtains the so-called band Jahn-Teller formula

$$C_\Gamma = C_\Gamma^0 - 2d^2 N_0[1 - e^{w/T}] \tag{6.3}$$

where C_Γ^0 is the back ground elastic constant, We adopted the back ground of C_Γ^0=AT+B with A= -0.0013 GPa/K and B = 96 GPa, d is the coupling constant, N_0 is the density of states at E_F. From the adjustable parameter d^2N_0 and band width w were evaluated as 20.8 for $2d^2N_0$, and 29.5 K for band width. The fitting of eq. (3) to the elastic softening in the experiments seems to be perfect, results are pictured in Fig. ??.

The large elastic anomalies compared with $Rh_{17}S_{15}$ have been reported in iron based superconductors $Ba(Fe_{1-x}Co_x)_2As_2$, A15 superconductor V_3Si and the Laves-phase superconductor $CeRu_2$ so far [56, 58, 59]. These anomalies have been ascribed to the large density of states at the Fermi energy. Fig. 6.11 describes the softening size of $Rh_{17}S_{15}$ with the iron based superconductor $Ba(Fe_{1-x}Co_x)_2As_2$ where x =0.084 and 0.098. Both samples show large elastic softening towards to low temperature and the softening behavior becomes to upturn at T_{sc}.

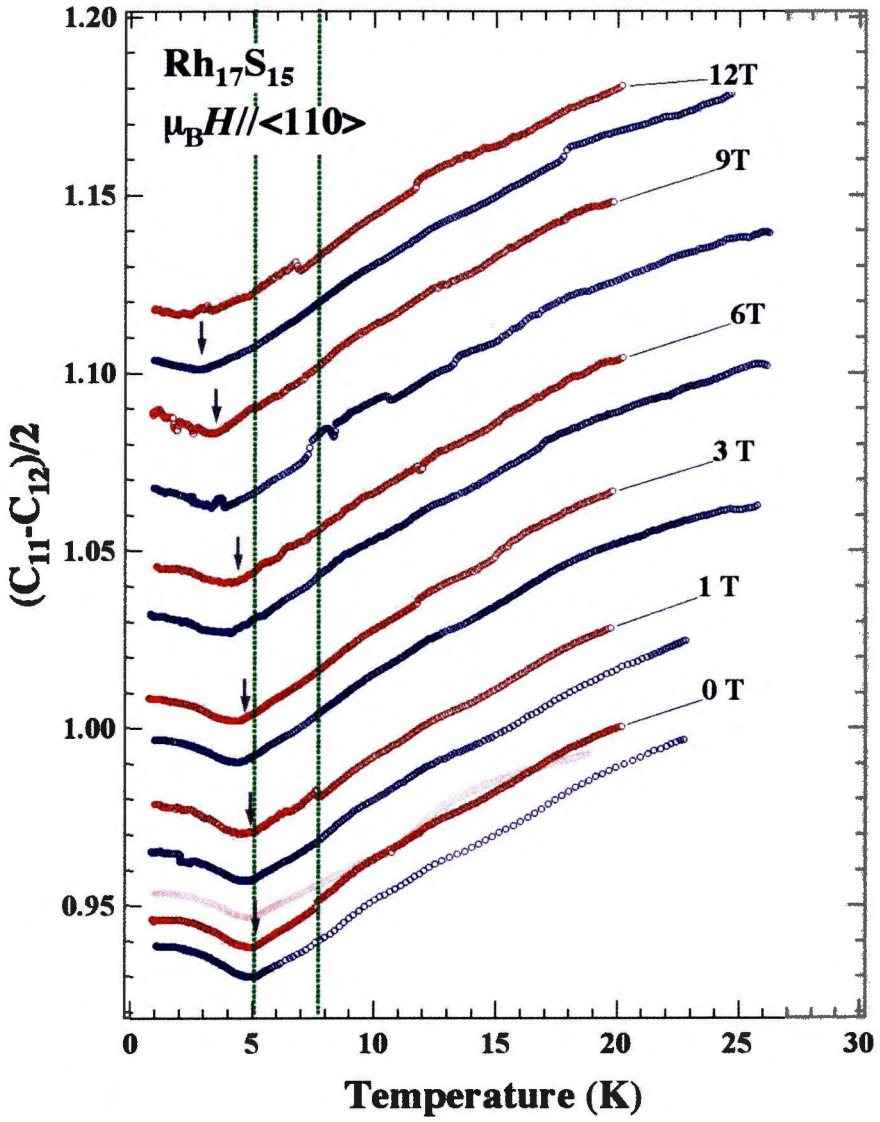

Figure 6.9: Field dependence of elastic constant C_{E} of the single crystal $Rh_{17}S_{15}$.

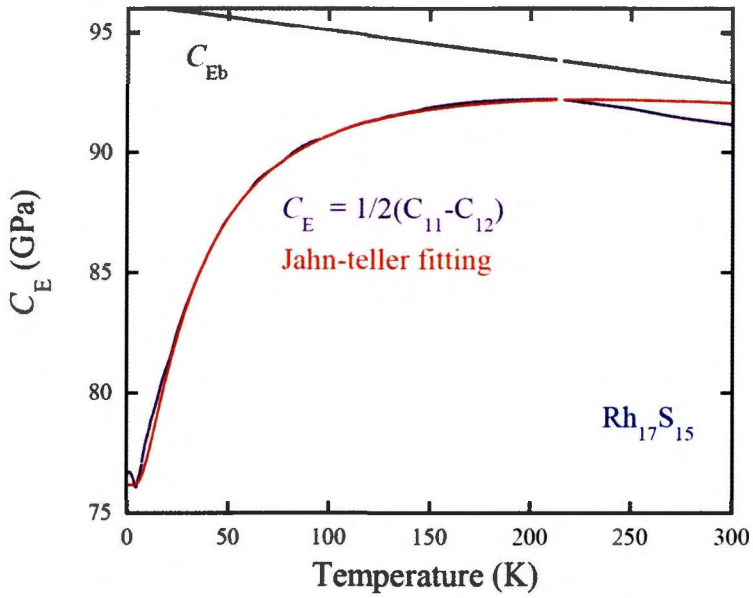

Figure 6.10: Fitting of C_E by the band Jahn-Teller effect. The adjustable parameters are the bandwidth W and the coupling constant d^2N_0.

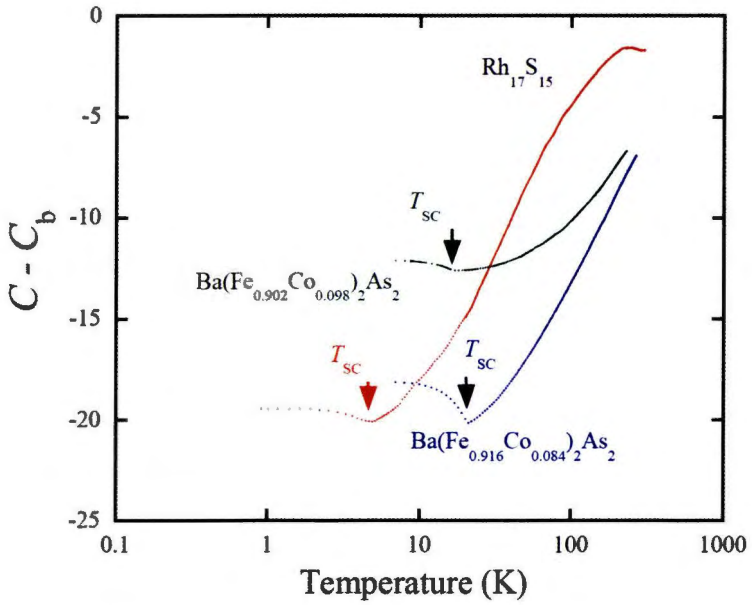

Figure 6.11: Compare the elastic constant of $Rh_{17}S_{15}$

Chapter 7

Conclusion

In this thesis we have reported elastic properties of iron-based superconductors $Ba(Fe_{1-x}Co_x)_2As_2$, and found the structural fluctuation in C_{66} associated with the structural (T_S) phase transition, and strange interlayer properties of $Ba(Fe_{1-x}Co_x)_2As_2$, by studying its elastic constant C_{33}.

In the studying of the elastic constant C_{66} structural quantum critical behavior was reported for $Ba(Fe_{1-x}Co_x)_2As_2$. The QCP behavior has also been reported by resistivity measurements and NMR of $Ba(Fe_{1-x}Co_x)_2As_2$[65]. The QCP behavior observed in NMR and elastic measurement is expected to be of the same origin. The elastic constant is not a sensitive measure of magnetism, but is a sensitive probe for orbitals (quadrupoles), in contrast to NMR. Our measurement entails an observation from the side of orbitals (quadrupoles). Our studies show that T_{sc} was enhanced near the QCP, and we found the correlation between the elastic softening and superconductivity.

Our results of C_{66} suggested the importance of orbital fluctuation in the emergence of superconductivity. Starting from our reports, many researchers have discussed the superconductivity based non the orbital fluctuations. On the other hand, the structural fluctuation leads to an in-plane order, and it possesses two-dimensional nature. However, an order is hard to occur in two-dimensional systems, so three-dimensionality is necessary for the occurrence of ordering. So we focused on our attention to the three-dimensional character of this system by measuring the elastic constant C_{33}. In this study, we found inter-layer fluctuation accompanying small lattice fluctuation. It does not stop below $T_{\rm S}$ and continues to $T_{\rm N}$. We obtained the Grüneisen parameter along c-axis. It becomes small near the QCP. This is very important information, because it is a reflection of $dT_{\rm sc}/d\varepsilon_{ZZ}$, which can be obtained only by elastic constant measurements. The amount of softening in C_{33} was enhanced near the QCP. In both results of C_{66} and C_{33}, we found the correlation of $T_{\rm sc}$ with the superconductivity, and the enhancement of $T_{\rm sc}$ near the QCP. This fact might be used as a probe for the discovery of high $T_{\rm sc}$ materials. We could find high $T_{\rm sc}$ materials through the exploration of materials showing elastic softening.

One question remains. Is the correlation between $T_{\rm sc}$ and $S_{66,cr}$ either a particular phenomenon existing only in $Ba(Fe_{1-x}Co_x)_2As_2$ or a universal one appearing in related materials including iron-based compounds? Huge elastic anomalies have been observed not only in iron-based superconductors, but also in famous practical materials of A15 compounds

such as Nb_3Sn and V_3Si, and Laves phase compound $CeRu_2$, so far. More recently in our studies we have found very large elastic softening in heavy fermion superconductor $Rh_{17}S_{15}$. On the other hand, elastic anomaly associated with the adjacent magnetic order has been observed in LSCO oxide superconductors, in addition to A15 compounds. How about the similarities and dissimilarities between the elastic anomalies in iron-based superconductors and those in other systems found in the past. In the case of Ba122, $E_{\rm JT}$ is very large, which is in the range of 20 50 K, whose amount is similar in A15 compounds. In contrast, the value of $E_{\rm JT}$ in LSCO is estimated to be small at about 1 K. In heavy fermion superconductor $Rh_{17}S_{15}$, the $E_{\rm JT}$ is estimated to be 8.5 K.

We are aware of that the materials, which show large elastic softening with large $E_{\rm JT}$, are all belonging to the substance group of transition metal compounds having a multi-orbital. It would be expected that possible high $T_{\rm sc}$ materials like iron-based superconductors would be discovered around them.

Chapter 8

Appendix

8.1 Analysis of elastic constants

We consider the elastic properties of a crystal viewed as a homogeneous continuous medium rather than as a periodic array of atoms. The continuum approximation is usually valid for elastic waves of wavelengths λ longer than 10^{-6} cm, which means for frequencies below 10^{11} or 10^{12} Hz. Some of the material below looks complicated because of the unavoidable multiplicity of subscripts on the symbols. The basic physical ideas are simple: we use Hook's law and Newton's second law. Hook's law states that in an elastic solid the strain is directly proportional to the stress. The law applies to small strains only. We say that we are in the nonlinear region when the strains are so large that Hook's law is no longer satisfied.

We specify the strain in terms of the components e_{xx}, e_{yy}, e_{zz}, e_{xy}, e_{yz}, e_{zx} which are defined below. We imagine that three orthogonal vectors $\hat{\mathbf{x}}$, $\hat{\mathbf{y}}$, $\hat{\mathbf{z}}$ of unit length are embedded securely in the unstrained solid, as

shown in Fig. 8.1. After uniform deformation of the solid has taken place, the axes are distorted in orientation and in length. In a uniform deformation each primitive cell of the crystal is deformed in the same way. The new axes $\mathbf{x}'$, $\mathbf{y}'$, $\mathbf{z}'$ may be written in terms of the old axes:

$$\begin{aligned}
\mathbf{x}' &= (1+\epsilon_{xx})\hat{\mathbf{x}} + \epsilon_{xy}\hat{\mathbf{y}} + \epsilon_{xz}\hat{\mathbf{z}} \\
\mathbf{y}' &= \epsilon_{yx}\hat{\mathbf{x}} + (1+\epsilon_{yy})\hat{\mathbf{y}} + \epsilon_{yz}\hat{\mathbf{z}} \\
\mathbf{z}' &= \epsilon_{zx}\hat{\mathbf{x}} + \epsilon_{zy}\hat{\mathbf{y}} + (1+\epsilon_{zz})\hat{\mathbf{z}}
\end{aligned} \tag{8.1}$$

The coefficient $\epsilon_{\alpha\beta}$ define the deformation; they are dimensionless and have values $\ll 1$ if the strain is small. The original axes were of unit length, but the new axes will not necessarily be of unit length. For example,

$$\mathbf{x}' \cdot \mathbf{x}' = 1 + 2\epsilon_{xx} + \epsilon_{xx}^2 + \epsilon_{xy}^2 + \epsilon_{xz}^2 \tag{8.2}$$

whence $x' \cong 1 + \epsilon_{xx} + \cdots$. The fractional changes of length of the $\hat{\mathbf{x}}, \hat{\mathbf{y}}$ and $\hat{\mathbf{z}}$ axes are $\epsilon_{xx}, \epsilon_{yy}, \epsilon_{zz}$, respectively, to the first order.

What is the effect of the deformation (8.1) on an atom originally at $\mathbf{r} = x\hat{\mathbf{x}} + y\hat{\mathbf{y}} + z\hat{\mathbf{z}}$? The origion is taken at some other atom. If the deformation is uniform, then after deformation the point will be at the position $\mathbf{r}' = x\mathbf{x}' + y\mathbf{y}' + z\mathbf{z}'$. This is obviously correct if we choose the $\hat{\mathbf{x}}$ axes such that $\mathbf{r} = x\hat{\mathbf{x}}$; then $\mathbf{r}' = x\mathbf{x}'$ by definition of $\mathbf{x}'$. The displacement $\mathbf{R}$ of the deformation is defined by

$$\mathbf{R} \equiv \mathbf{r}' - \mathbf{r} = x(\mathbf{x}' - \hat{\mathbf{x}}) + y(\mathbf{y}' - \hat{\mathbf{y}}) + z(\mathbf{z}' - \hat{\mathbf{z}}), \tag{8.3}$$

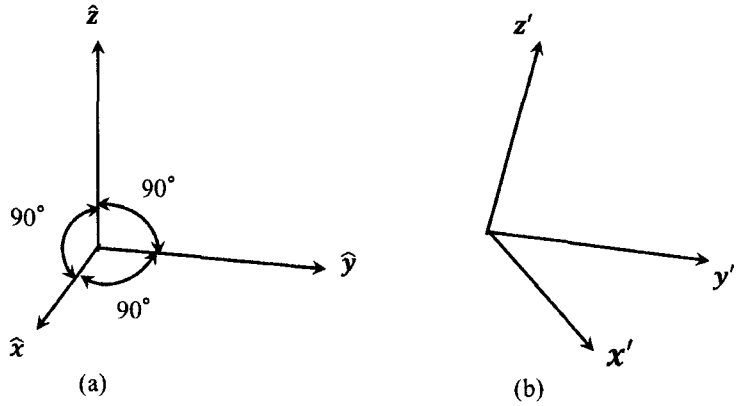

Figure 8.1: (Color online) (a) The orthogonal unit axes in the unstrained state. (b) Deformed in the strained state

or, from equation (8.1),

$$\mathbf{R}(\mathbf{r}) \equiv (x\epsilon_{xx}+y\epsilon_{yx}+z\epsilon_{zx})\mathbf{x}'+(x\epsilon_{xy}+y\epsilon_{yy}+z\epsilon_{zy})\mathbf{y}'+(x\epsilon_{xz}+y\epsilon_{yz}+z\epsilon_{zz})\mathbf{z}'. \tag{8.4}$$

This may be written in a more general form by introducing components of displacement u, v, w such that the displacement is given by

$$\mathbf{R}(\mathbf{r}) = u(\mathbf{r})\hat{\mathbf{x}} + v(\mathbf{r})\hat{\mathbf{y}} + w(\mathbf{r})\hat{\mathbf{z}}. \tag{8.5}$$

If the deformation is nonuniform we must relate u, v, w to the local strain. We take the origin of $\mathbf{r}$ close to the region of interest; then comparison of (8.4) and (8.5) gives, by Taylor series expansion of $\mathbf{R}$ using $\mathbf{R}(0) = 0$,

$$x\epsilon_{xx} = x\frac{\partial u}{\partial x}; \qquad y\epsilon_{yx} = y\frac{\partial u}{\partial y}; \qquad etc. \tag{8.6}$$

It is usual to work with coefficients $e_{\alpha\beta}$ rather than $\epsilon_{\alpha\beta}$. We define the strain components e_{xx}, e_{yy}, e_{zz} by the relations

$$e_{xx} \equiv \epsilon_{xx} = \frac{\partial u}{\partial x}; \qquad e_{yy} \equiv \epsilon_{yy} = \frac{\partial v}{\partial y}; \qquad e_{zz} \equiv \epsilon_{zz} = \frac{\partial w}{\partial z}; \tag{8.7}$$

using (8.6). The other strain components e_{xy}, e_{yz}, e_{zx} are defined in terms of the changes in angle between the axes: using (8.1) we may define

$$\begin{aligned} e_{xy} &\equiv \mathbf{x}' \cdot \mathbf{y}' \cong \epsilon_{yx} + \epsilon_{xy} = \frac{\partial u}{\partial y} + \frac{\partial v}{\partial x}; \\ e_{yz} &\equiv \mathbf{y}' \cdot \mathbf{z}' \cong \epsilon_{zy} + \epsilon_{yz} = \frac{\partial v}{\partial z} + \frac{\partial w}{\partial y}; \\ e_{zx} &\equiv \mathbf{z}' \cdot \mathbf{x}' \cong \epsilon_{zx} + \epsilon_{xz} = \frac{\partial u}{\partial z} + \frac{\partial w}{\partial x}. \end{aligned} \tag{8.8}$$

8.2 Dilation

The fractional increase of volume associated with a deformation is called the dilation. The dilation is negative for hydrostatic pressure. The unit cube of edges $\hat{\mathbf{x}}, \hat{\mathbf{y}}, \hat{\mathbf{z}}$ has a volume after deformation of

$$V' = \mathbf{x}' \cdot \mathbf{y}' \times \mathbf{z}' \tag{8.9}$$

by virtue of a well-known result for the volume of a parallel piped having edges $\mathbf{x}', \mathbf{y}', \mathbf{z}'$. From equation (8.1) we have

$$\mathbf{x}' \cdot \mathbf{y}' \times \mathbf{z}' = \begin{vmatrix} 1+\epsilon_{xx} & \epsilon_{xy} & \epsilon_{xz} \\ \epsilon_{yx} & 1+\epsilon_{yy} & \epsilon_{yz} \\ \epsilon_{zx} & \epsilon_{zy} & 1+\epsilon_{zz} \end{vmatrix} \cong 1 + e_{xx} + e_{yy} + e_{zz}. \tag{8.10}$$

Products of two strain components have been neglected. The dilation δ is then given by

$$\delta \equiv \frac{V' - V}{V} \cong e_{xx} + e_{yy} + e_{zz}. \tag{8.11}$$

8.3 Stress Components

The force acting on a unit area in the solid is defined as the stress. There are nine stress components: $X_x, X_y, X_z, Y_x, Y_y, Y_z, Z_x, Z_y, Z_z$. The capital letter indicates the direction of the force, and the subscript indicates the normal to the plane to which the force is applied. In Fig. 8.2 the stress components X_x represents a force applied in the x direction to a unit area of a plane whose normal lies in the x direction; the stress component X_y represents a force applied in the x direction to a unit area of a plane whose normal lies in the y direction. The number of independent stress components is reduced from nine to six by applying to an elementary cube (as in Fig. 8.3) the condition that the angular acceleration vanish, and hence that the total torque must be zero. It follows that

$$Y_z = Z_y; \qquad Z_x = X_z; \qquad X_y = Y_x \tag{8.12}$$

The six independent stress components may be taken as $X_x, Y_y, Z_z, Y_z, Z_x, X_y$. Stress components have the dimensions of force per unit area or energy per unit volume. The strain components are ratios of lengths and are dimensionless.

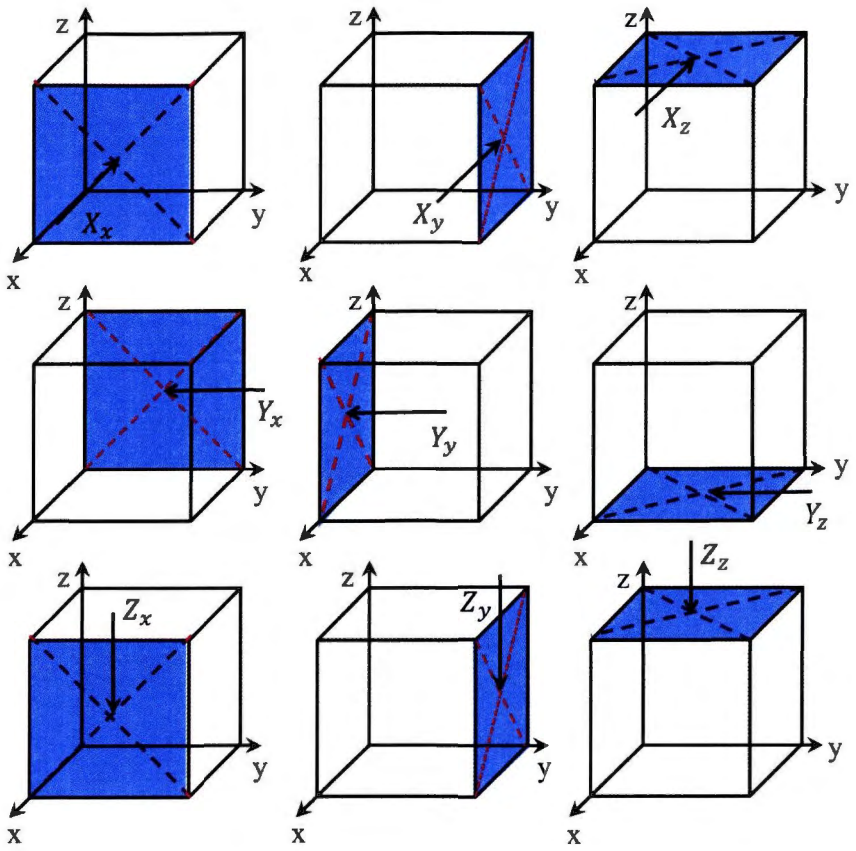

Figure 8.2: (Color online) Stress components force applied in to a unit area of a plane whose normal lies.

8.4 Elastic compliance and stiffness constants

Hooke's law states that for sufficiently small deformations the strain is directly proportional to the stress, so that the strain components are

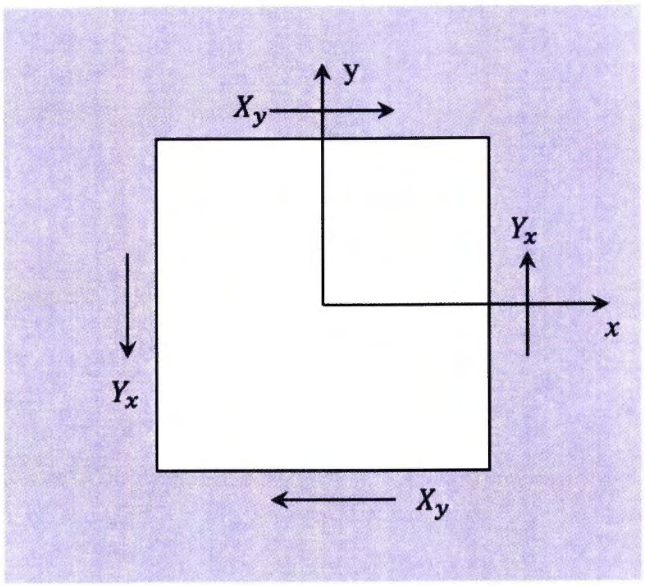

Figure 8.3: (Color online) Stress components force applied in to a unit area of a plane whose normal lies.

linear functions of the stress components:

$$
\begin{aligned}
e_{xx} &= S_{11}X_x + S_{12}Y_y + S_{13}Z_z + S_{14}Y_z + S_{15}Z_x + S_{16}X_y; \\
e_{yy} &= S_{21}X_x + S_{22}Y_y + S_{23}Z_z + S_{24}Y_z + S_{25}Z_x + S_{26}X_y; \\
e_{zz} &= S_{31}X_x + S_{32}Y_y + S_{33}Z_z + S_{34}Y_z + S_{35}Z_x + S_{36}X_y; \\
e_{yz} &= S_{41}X_x + S_{42}Y_y + S_{43}Z_z + S_{44}Y_z + S_{45}Z_x + S_{46}X_y; \\
e_{zx} &= S_{51}X_x + S_{52}Y_y + S_{53}Z_z + S_{54}Y_z + S_{55}Z_x + S_{56}X_y; \\
e_{xy} &= S_{61}X_x + S_{62}Y_y + S_{63}Z_z + S_{64}Y_z + S_{65}Z_x + S_{66}X_y;
\end{aligned}
\tag{8.13}
$$

$$
\begin{aligned}
X_x &= C_{11}e_{xx} + C_{12}e_{yy} + C_{13}e_{zz} + C_{14}e_{yz} + C_{15}e_{zx} + C_{16}e_{xy};\\
Y_y &= C_{21}e_{xx} + C_{22}e_{yy} + C_{23}e_{zz} + C_{24}e_{yz} + C_{25}e_{zx} + C_{26}e_{xy};\\
Z_z &= C_{31}e_{xx} + C_{32}e_{yy} + C_{33}e_{zz} + C_{34}e_{yz} + C_{35}e_{zx} + C_{36}e_{xy}; \qquad (8.14)\\
Y_z &= C_{41}e_{xx} + C_{42}e_{yy} + C_{43}e_{zz} + C_{44}e_{yz} + C_{45}e_{zx} + C_{46}e_{xy};\\
Z_x &= C_{51}e_{xx} + C_{52}e_{yy} + C_{53}e_{zz} + C_{54}e_{yz} + C_{55}e_{zx} + C_{56}e_{xy};\\
X_y &= C_{61}e_{xx} + C_{62}e_{yy} + C_{63}e_{zz} + C_{64}e_{yz} + C_{65}e_{zx} + C_{66}e_{xy};
\end{aligned}
$$

The quantities S_{11}, $S_{12}\cdots$ are called elastic compliance constants or elastic constants; the quantities C_{11}, $C_{12}\cdots$ are called the elastic stiffness constants or moduli of elasticity. The S's have the dimensions of [area]/[force] or [volume]/[energy]. The C's have the dimensions of [force]/[area] or [energy]/[volume].

8.5 Elastic energy density

The 36 constants in (8.4) or in (8.4) may be reduced by several considerations. The elastic energy density U is a quadratic function of the strains, in the approximation of Hooke's law (recall the expression for the energy of a stretched spring). Thus we may write

$$
U = \frac{1}{2}\sum_{\lambda=1}^{6}\sum_{\mu=1}^{6}\tilde{C}_{\lambda\mu}e_{\lambda}e_{\mu} \qquad (8.15)
$$

where the indicts 1 through 6 are defined as:

$$
1 \equiv xx; \quad 2 \equiv yy; \quad 3 \equiv zz; \quad 4 \equiv yz; \quad 5 \equiv zx; \quad 6 \equiv xy; \qquad (8.16)
$$

The $\tilde{C}'s$ are related to the $\tilde{C}'s$ of (8.4), as in (8.18) below.

The stress components are found from the derivative of U with respect to the associated strain components. This result follows from the definition of potential energy. Consider the stress X_x applied to one face of a unit cube, the opposite face being held at rest:

$$X_x = \frac{\partial U}{\partial e_{xxz}} \equiv \frac{\partial U}{\partial e_1} = \tilde{C}_{11}e_1 + \frac{1}{2}\sum_{\beta=1}^{6}(\tilde{C}_{1\beta} + \tilde{C}_{\beta 1})e_\beta. \tag{8.17}$$

Note that only the combination $\frac{1}{2}(\tilde{C}_{\alpha\beta} + \tilde{C}_{\beta\alpha})$ enters the stress-strain relations. It follows that the elastic stiffness constants are symmetrical:

$$C_{\alpha\beta} = \frac{1}{2}(\tilde{C}_{\alpha\beta} + \tilde{C}_{\beta\alpha}) = C_{\beta\alpha} \tag{8.18}$$

Thus the thirty six elastic stiffness constants are reduced to twenty-one.

8.6 Elastic stiffness constants of cubic crystals

The number of independent elastic stiffness constants is reduced further if the crystal possess symmetry elements. We now show that in cubic crystals there are only three independent stiffness constants.

We assert that the elastic energy density of a cubic crystal is

$$U = \frac{1}{2}C_{11}(e_{xx}^2+e_{yy}^2+e_{zz}^2)+\frac{1}{2}C_{44}(e_{yz}^2+e_{zx}^2+e_{xy}^2)+C_{12}(e_{yy}e_{zz}+e_{zz}e_{xx}+e_{xx}e_{yy}), \tag{8.19}$$

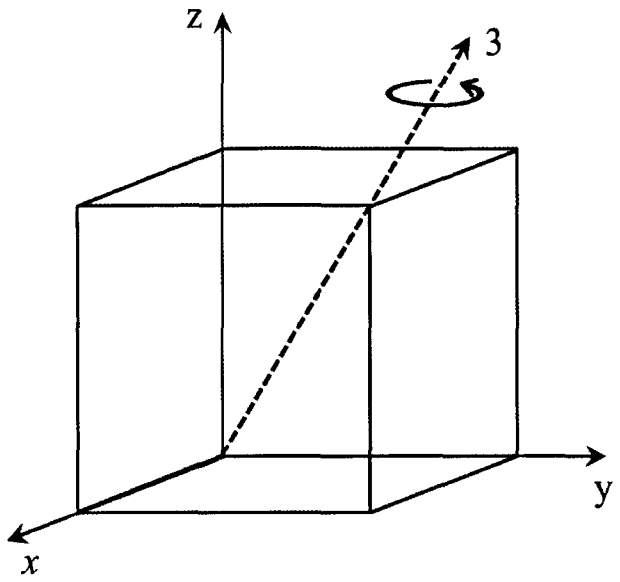

Figure 8.4: (Color online) Rotation by $2\pi/3$ about the axis marked 3 changes $x \to y$; $y \to z$; and $z \to x$..

and that no other quadratic terms occur; that is,

$$(e_{xx}e_{yy} + \cdots); \qquad (e_{yz}e_{zx} + \cdots); \qquad (e_{xx}e_{yz} + \cdots); \tag{8.20}$$

do not occur.

The minimum symmetry requirement for a cubic structure is the existence of four three-fold rotation axes. The axes in the [111] and quivalent directions (Fig. 8.4). The effect of rotation of $2\pi/3$ about these four axes is to interchang the x, y, z axes according to the schemes

$$\begin{aligned} x \to y \to z \to x; \qquad -x \to z \to y \to -x; \\ x \to z \to -y \to x; \qquad -x \to y \to z \to -x; \end{aligned} \tag{8.21}$$

according to the axis chosen. Under the first of these schemes, for example,

$$e_{xx}^2 + e_{yy}^2 + e_{zz}^2 \to e_{yy}^2 + e_{zz}^2 + e_{xx}^2 \tag{8.22}$$

and similarly for the other terms in parentheses in (8.19). Thus (8.19) is invariant under the operations considered. But each of the terms exhibited in (8.20) is odd in one or more indices. A rotation in the set (8.21) can be found which will change the sign of the term, because $e_{xy} = -e_{x(-y)}$, for example. Thus the terms (8.20) are not invariant under the required operations.

It remains to verify that the numerical factors in (8.19) are coorect. By (8.17),

$$\frac{\partial U}{\partial e_{xx}} = X_x = C_{11}e_{xx} + C_{12}(e_{yy} + e_{zz}) \tag{8.23}$$

The appearance of $C_{11}e_{xx}$ agrees with (8.4). On further comparison, we see that

$$C_{12} = C_{13}; \qquad C_{14} = C_{15} = C_{16} = 0. \tag{8.24}$$

Further, from (8.19),

$$\frac{\partial U}{\partial e_{xy}} = X_y = C_{44}e_{xy}; \tag{8.25}$$

on comparison with (8.4) we have

$$C_{61} = C_{62} = C_{63} = C_{64} = C_{65} = 0; \quad C_{66} = C_{44}. \tag{8.26}$$

Thus from (8.19) we find that the array of values of the elastic stiffness

constants is reduced for a cubic crystal to the matrix

	e_{xx}	e_{yy}	e_{zz}	e_{yz}	e_{zx}	e_{xy}
X_x	C_{11}	C_{12}	C_{12}	0	0	0
Y_y	C_{12}	C_{11}	C_{12}	0	0	0
Z_z	C_{12}	C_{12}	C_{11}	0	0	0
Y_z	0	0	0	C_{44}	0	0
Z_x	0	0	0	0	C_{44}	0
X_y	0	0	0	0	0	C_{44}

(8.27)

For cubic crystals the stiffness and compliance constants are related by

$$C_{14} = 1/S_{44};\quad C_{11} - C_{12} = (S_{11} - S_{12})^{-1};\quad C_{11} + 2C_{12} = (S_{11} + 2S_{12})^{-1} \tag{8.28}$$

These relations follow on evaluating the inverse matrix to (8.27)

8.7 Elastic waves in cubic crystals

By considering as in Fig. 8.5 the forces acting on an element of volume in the crystal we obtain the equation of motion in the x direction

$$\rho\frac{\partial^2 u}{\partial t^2} = \frac{\partial X_x}{\partial x} + \frac{\partial X_y}{\partial y} + \frac{\partial X_z}{\partial z}; \tag{8.29}$$

here ρ is the density and u is the displacement in the x direction. There are similar equations for the y and z directions. From (8.4) and (8.27) it follows that for a cubic crystal

$$\rho\frac{\partial^2 u}{\partial t^2} = C_{11}\frac{\partial e_{xx}}{\partial x} + C_{12}(\frac{\partial e_{yy}}{\partial x} + \frac{\partial e_{zz}}{\partial x}) + C_{44}(\frac{\partial e_{xy}}{\partial y} + \frac{\partial e_{zx}}{\partial z}); \qquad (8.30)$$

here the x, y, z directions are parallel to the cube edges. Using the definitions (8.7) and (8.1) of the strain components we have

$$\rho\frac{\partial^2 u}{\partial t^2} = C_{11}\frac{\partial^2 u}{\partial x^2} + C_{44}(\frac{\partial^2 u}{\partial y^2} + \frac{\partial^2 u}{\partial z^2}) + (C_{12} + C_{44})(\frac{\partial^2 v}{\partial x \partial y} + \frac{\partial w}{\partial x \partial z}); \quad (8.31)$$

where u, v, w are the components of the displacement $\boldsymbol{R}$ as defined by (8.5).

The corresponding equations of motion for $\frac{\partial^2 v}{\partial t^2}$ and $\frac{\partial^2 w}{\partial t^2}$ are found directly from (8.31) by symmetry:

$$\rho\frac{\partial^2 v}{\partial t^2} = C_{11}\frac{\partial^2 v}{\partial y^2} + C_{44}(\frac{\partial^2 v}{\partial x^2} + \frac{\partial^2 v}{\partial z^2}) + (C_{12} + C_{44})(\frac{\partial u}{\partial x \partial y} + \frac{\partial w}{\partial y \partial z}); \qquad (8.32)$$

$$\rho\frac{\partial^2 w}{\partial t^2} = C_{11}\frac{\partial^2 w}{\partial z^2} + C_{44}(\frac{\partial^2 w}{\partial x^2} + \frac{\partial^2 w}{\partial y^2}) + (C_{12} + C_{44})(\frac{\partial u}{\partial x \partial z} + \frac{\partial v}{\partial y \partial z}); \qquad (8.33)$$

we now look for simple special solutions of these equations.

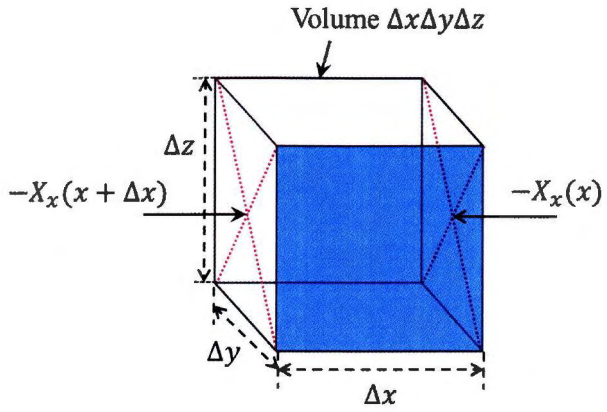

Figure 8.5: (Color online) Cube of volume $\Delta x \Delta y \Delta z$ acted on by a stress $-X_x(x)$ on the face at x, and $X_x(x + \Delta x) = X_x(x) + \frac{\partial X_x}{\partial x}\Delta x$.

8.8 Waves in the [100] direction

One solution of (8.31) si given by a longitudinal wave

$$u = u_0 exp[i(Kx - \omega t)] \tag{8.34}$$

where u is the x component of the particle displacement. Both the wavevector and the particle motion are long the x cube edge. Here $K = 2\pi/\lambda$ is the wave vector and $\omega = 2\pi v$ is the angular frequency. If we substitute (8.35) into (8.31) we find

$$\omega^2 \rho = C_{11} K^2 \tag{8.35}$$

thus the velocity ω/K of the longitudinal wave in the [100] direction is

$$v_s = v\lambda = \omega/K = (C_{11}/\rho)^{1/2}. \tag{8.36}$$

Consider a transverse or shear wave with the wavevector along the x cube edge and with the particle displacement v in the y direction:

$$v = v_0 exp[i(Kx - \omega t). \tag{8.37}$$

On substitution in (8.33) this gives the dispersion relation

$$\omega^2 \rho = C_{44} K^2; \tag{8.38}$$

thus the velocity ω/K of the transverse wave in the [100] direction is

$$v_s = (C_{44}/\rho)^{1/2}. \tag{8.39}$$

The identical velocity is obtained if the particle displacement is in the z direction. Thus for $\boldsymbol{K}$ parallel to [100] the two independent shear waves have equal velocities. This is not true for $\boldsymbol{K}$ in a general direction in the crystal.

8.9 Wave in the [110] direction

There is a special interest in waves that propagate in a face diagonal direction of a cubic crystal, because the three elastic constants can be found simply from the three propagation velocities in this direction. Consider a shear wave that propagates in the xy plane with particle

displacement w in the z direction

$$w = w_0 exp[i(K_x x + k_y y) - \omega t)], \tag{8.40}$$

whence (**??**) gives

$$\omega^2 \rho = C_{44}(K_x^2 + K_y^2) = C_{44} K^2, \tag{8.41}$$

independent of propagation direction in the plane.

Consider other waves that propagate in the xy plane with particle motion in the xy plane: let

$$u = u_0 exp[i(K_x x + K_y y - \omega t)]; \quad v = v_0 exp[i(K_x x + K_y y - \omega t)]. \tag{8.42}$$

From (8.31) and (8.33),

$$\begin{aligned} \omega^2 \rho u &= (C_{11} K_x^2 + C_{44} K_y^2) u + (C_{12} + C_{44}) K_x K_y v; \\ \omega^2 \rho v &= (C_{11} K_y^2 + C_{44} K_x^2) v + (C_{12} + C_{44}) K_x K_y u; \end{aligned} \tag{8.43}$$

This pair of equations has a particularly simple solution for a wave in the [110] direction, for which $K_x = K_y = K/\sqrt{2}$. The condition for a solution is that the determinant of the coefficients of u and v in (8.44) should equal zero:

$$\begin{vmatrix} -\omega^2 \rho + \frac{1}{2}(C_{11} + C_{44}) K^2 & \frac{1}{2}(C_{12} + C_{44}) K^2 \\ \frac{1}{2}(C_{12} + C_{44}) K^2 & -\omega^2 \rho + \frac{1}{2}(C_{11} + C_{44}) K^2 \end{vmatrix} \tag{8.44}$$

This equation has the roots

$$\omega^2\rho = \frac{1}{2}(C_{11} + C_{12} + 2C_{44})K^2; \quad \omega^2\rho = \frac{1}{2}(C_{11} - C_{12})K^2 \tag{8.45}$$

The first root describes longitudinal wave; the second root describes a shear wave. How do we determine the direction of particle displacement? The first root when substituted into the upper equation of (8.44) gives

$$\frac{1}{2}(C_{11}+C_{12}+2C_{44})K^2u = \frac{1}{2}(C_{11}+C_{44})K^2u+\frac{1}{2}(C_{12}+C_{44})K^2v, \tag{8.46}$$

whence the displacement components satisfy $u = v$. Thus the particle displacement is along [110] and parallel to the $\boldsymbol{K}$ vector (Fig. 8.6). The second root of (8.45) when substituted into the upper equation of (8.44) gives

$$\frac{1}{2}(C_{11} - C_{12})K^2u = \frac{1}{2}(C_{11} + C_{44})K^2u + \frac{1}{2}(C_{12} + C_{44})K^2v, \tag{8.47}$$

whence $u = -v$. The particle displacement is along $[1\bar{1}0]$ and perpendicular to the $\boldsymbol{K}$ vector.

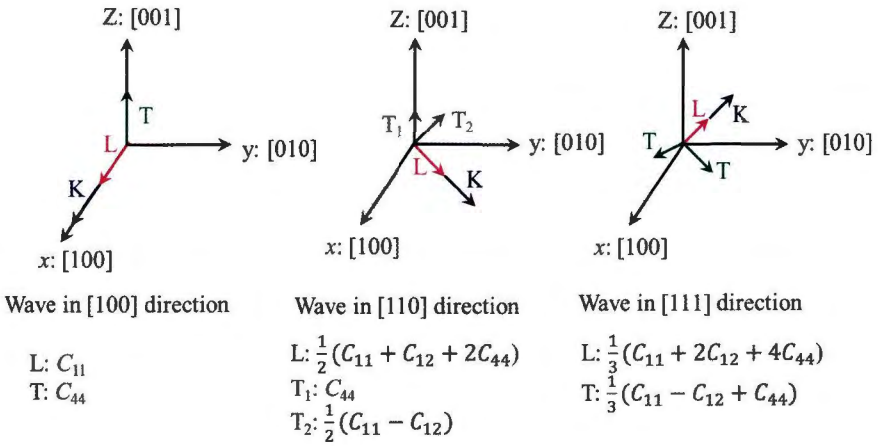

Figure 8.6: (Color online) Effective elastic constants for the three modes of elastic waves in the principal propagation directions in cubic crystals.

8.10 Elastic stiffness constants of tetragonal crystals

The minimum symmetry requirement for a tetragonal structure is the existence of four four-fold rotation axes. A rotation through 90° about z has the effect $x \to y \to -x, z \to z$. Applying this operation to the energy density (8.15), and equating the coefficients of the corresponding terms in (8.15) and in the transformed expression, we find the following conditions on the elastic constants:

$$\begin{gathered} C_{11} = C_{12},\ C_{44} = C_{55},\ C_{13} = C_{23},\ C_{16} = -C_{26},\ C_{34} = -C_{35}, \\ C_{14} = C_{25} = C_{15} = C_{24} = C_{36} = C_{45} = C_{46} = C_{56} = 0 \end{gathered} \tag{8.48}$$

This reduce the number of independent elastic constants to eight and elastic energy density becomes

$$\begin{aligned} U = \frac{1}{2}(e_{xx}^2 + e_{yy}^2) + \frac{1}{2}C_{33}e_{xx}^2 + C_{12}e_{xx}e_{yy} + C_{13}(e_{xx} + e_{yy})e_{zz} \\ + C_{16}(e_{xx} - e_{yy})e_{xy} + C_{34}(e_{yz} - e_{zx})e_{zz} \\ + \frac{1}{2}C_{44}(e_{yz}^2 + e_{zx}^2) + \frac{1}{2}C_{66}e_{xy}^2 \end{aligned} \tag{8.49}$$

Tetragonal structure also includes two-fold semmetry about the x or y axis. Consider a rotation through π about z axis, which has the effect $y \to -y, z \to -z, x \to x$. Applying this on the energy density (8.50), we find that all terms remain invariant except the two involving coefficients C_{16} and C_{34}, which must vanish. The final form of the energy density is then

$$\begin{aligned} U = \frac{1}{2}C_{11}(e_{xx}^2 + e_{yy}^2) + \frac{1}{2}C_{33}e_{xx}^2 + C_{12}e_{xx}e_{yy} \\ + C_{13}(e_{xx} + e_{yy})e_{zz} + \frac{1}{2}C_{44}(e_{yz}^2 + e_{zx}^2) \\ + \frac{1}{2}C_{66}e_{xy}^2 \end{aligned} \tag{8.50}$$

The stress components are found from the derivative of U with respect to the associated strain component. This result follows from the definition of potential energy. Consider the stress X_x applied to one face of a unit,

the opposite face being held at rest so that we can obtain

$$\frac{\partial U}{\partial e_{xx}} = X_x = C_{11}e_{xx} + C_{12}e_{yy} + C_{13}e_{zz} \tag{8.51}$$

$$\frac{\partial U}{\partial e_{yy}} = Y_y = C_{12}e_{xx} + C_{11}e_{yy} + C_{13}e_{zz} \tag{8.52}$$

$$\frac{\partial U}{\partial e_{zz}} = Z_z = C_{33}e_{zz} + C_{13}(e_{xx} + e_{yy}) \tag{8.53}$$

$$\frac{\partial U}{\partial e_{xy}} = X_y = C_{66}e_{xy} \tag{8.54}$$

$$\frac{\partial U}{\partial e_{yz}} = Y_z = C_{44}e_{yz} \tag{8.55}$$

$$\frac{\partial U}{\partial e_{zx}} = Z_x = C_{44}e_{zx} \tag{8.56}$$

$$\tag{8.57}$$

It can be seen that any other transformation of tetragonal structure leave the bilinear form (8.57) invariant, so that there is no further simplification. A tetragonal crystal has six independent elastic constants, and matrix of elastic constants reduces the form

$$\begin{bmatrix} X_x \\ Y_y \\ Z_z \\ Y_z \\ Z_x \\ X_y \end{bmatrix} = \begin{bmatrix} C_{11} & C_{12} & C_{13} & 0 & 0 & 0 \\ C_{12} & C_{11} & C_{13} & 0 & 0 & 0 \\ C_{13} & C_{13} & C_{33} & 0 & 0 & 0 \\ 0 & 0 & 0 & 0 & 0 & 0 \\ 0 & 0 & 0 & 0 & 0 & 0 \\ 0 & 0 & 0 & 0 & 0 & 0 \end{bmatrix} \begin{bmatrix} e_{xx} \\ e_{yy} \\ e_{zz} \\ e_{yz} \\ e_{zx} \\ e_{xy} \end{bmatrix} \tag{8.58}$$

8.11 Elastic waves in tetragonal crystal

The force has been indicate by the mass of the tetragonal and times the components of the acceleration in the x direction. The mass is $\rho\Delta x\Delta y\Delta z$, and the acceleration is $\frac{\partial^2 u}{\partial t^2}$, so it takes

$$\rho\frac{\partial^2 u}{\partial t^2} = C_{11}\frac{\partial e_{xx}}{\partial x} + C_{12}\frac{\partial e_{yy}}{\partial x} + C_{13}\frac{\partial e_{zz}}{\partial x} + C_{66}\frac{\partial e_{xy}}{\partial y} + C_{44}\frac{\partial e_{zx}}{\partial z} \tag{8.59}$$

here the strain components are

$$\begin{aligned} e_{xx} &= \frac{\partial u}{\partial x}; \quad e_{yy} = \frac{\partial v}{\partial y}; \quad e_{zz} = \frac{\partial w}{\partial z}; \\ e_{yz} &= \frac{\partial v}{\partial z} + \frac{\partial w}{\partial y}; \quad e_{zx} = \frac{\partial u}{\partial z} + \frac{\partial w}{\partial x}; \quad e_{xy} = \frac{\partial u}{\partial y} + \frac{\partial v}{\partial x}; \end{aligned} \tag{8.60}$$

from this formula we can get

$$\rho\frac{\partial^2 u}{\partial t^2} = C_{11}\frac{\partial^2 u}{\partial x^2} + C_{66}(\frac{\partial^2 u}{\partial y^2} + C_{44}\frac{\partial^2 u}{\partial z^2} + (C_{12}+C_{66})\frac{\partial^2 v}{\partial x\partial y} + (C_{13}+C_{44})\frac{\partial^2 w}{\partial z\partial x} \tag{8.61}$$

The corresponding equations of motion for $\frac{\partial^2 v}{\partial t^2}$ and $\frac{\partial^2 w}{\partial t^2}$ are

$$\rho\frac{\partial^2 v}{\partial t^2} = C_{11}\frac{\partial^2 v}{\partial y^2} + C_{66}(\frac{\partial^2 v}{\partial x^2} + C_{44}\frac{\partial^2 v}{\partial z^2} + (C_{12}+C_{44})\frac{\partial^2 w}{\partial y\partial z} + (C_{12}+C_{66})\frac{\partial^2 u}{\partial x\partial y} \tag{8.62}$$

$$\rho\frac{\partial^2 w}{\partial t^2} = C_{44}\frac{\partial^2 w}{\partial x^2} + C_{44}(\frac{\partial^2 w}{\partial y^2} + C_{33}\frac{\partial^2 w}{\partial z^2} + (C_{13}+C_{44})\frac{\partial^2 u}{\partial x\partial z} + (C_{13}+C_{44})\frac{\partial^2 v}{\partial y\partial x} \tag{8.63}$$

We now look for simple special solutions of these equations.

8.12 Waves in the [100] direction

On the solution (8.31) is given by a longitudinal wave

$$u(K) = u_0 exp[i(Kx - \omega t), \tag{8.64}$$

where u is the x component of the particle displacement. Both the wavevector and the particle motion are along the x direction. Here $K = 2\pi/\lambda$ is the wave vector and $\omega = 2\pi v$ is the angular frequency. If we substitude (8.35) into (8.31) we find

$$\omega^2 \rho = C_{11} K^2 \tag{8.65}$$

thus the velocity ω/K of a longitudinal wave in the [100] direction is

$$v_L = \nu\lambda = \omega/K = \sqrt{C_{11}/\rho}. \tag{8.66}$$

Consider a transverse or shear wave with the wave vector along the x direction and with the particle displacement v in the y direction:

$$v(K) = v_0 exp[i(Kt - \omega t)] \tag{8.67}$$

On the substitution in to (8.31) this gives the dispersion relation

$$\omega^2 \rho = C_{66} K^2; \tag{8.68}$$

thus the velocity ω/K of a transverse wave in [100] direction is

$$v_T = \sqrt{(C_{66}/\rho)} \tag{8.69}$$

If the particle displacement v in the z direction, we find the velocity ω/K of a transverse wave in the [100] direction is

$$v_T = \sqrt{(C_{44}/\rho)} \tag{8.70}$$

8.13 Waves in the [001] direction

On the solution (8.31) is given by a longitudinal wave

$$w(K) = w_0 exp[i(Kz - \omega t)], \tag{8.71}$$

where w is the z component of the particle displacement. Both the wave vector and the particle motion are along the z direction. Here $K = 2\pi/\lambda$ is the wave vector and $\omega = 2\pi v$ is the angular frequency. If we substitute (8.35) into (8.31) we find

$$\omega^2 \rho = C_{33} K^2 \tag{8.72}$$

thus the velocity ω/K of a longitudinal wave in the [001] direction is

$$w_L = \nu\lambda = \omega/K = \sqrt{C_{33}/\rho}. \tag{8.73}$$

Consider a transverse or shear wave with the wave vector along the z direction and with the particle displacement u in the x direction:

$$u(K) = u_0 exp[i(Kt - \omega t)] \tag{8.74}$$

On the substitution in to (8.33) this gives the dispersion relation

$$\omega^2 \rho = C_{44} K^2; \tag{8.75}$$

thus the velocity ω/K of a transverse wave in [001] direction is

$$u_T = \sqrt{(C_{44}/\rho)} \tag{8.76}$$

If the particle displacement v in the y direction, we find the velocity ω/K of a transverse wave in the [001] direction is

$$v_T = \sqrt{(C_{44}/\rho)} \tag{8.77}$$

8.14 Waves in the [110] direction

Consider a shear wave that propagates in the xy plane with particle displacement w in the z direction

$$w = w_0 exp[i(K_x x + K_y y - \omega t)] \tag{8.78}$$

if we substitute this into (8.68) we find

$$\omega^2\rho = C_{44}K^2 \tag{8.79}$$

independent of propagation direction in the plane.

Consider other waves that propagates in the xy plane with particle motion in the xy plane: let

$$u = u_0 exp[i(K_x x + K_y y - \omega t)] \tag{8.80}$$

$$v = v_0 exp[i(K_x x + K_y y - \omega t)] \tag{8.81}$$

from (8.31) and (8.35),

$$\omega^2\rho u = \frac{1}{2}(C_{11} + C_{66})K^2 u + \frac{1}{2}(C_{12} + C_{66})K^2 v \tag{8.82}$$

$$\omega^2\rho v = \frac{1}{2}(C_{12} + C_{66})K^2 u + \frac{1}{2}(C_{11} + C_{66})K^2 v \tag{8.83}$$

The condition for this solution is that the determinant of the coefficients of u and v in (8.44) should be zero:

$$\begin{vmatrix} -\omega^2\rho + \frac{1}{2}(C_{11} + C_{66})K^2 & \frac{1}{2}(C_{12} + C_{66})K^2 \\ \frac{1}{2}(C_{12} + C_{66})K^2 & -\omega^2\rho + \frac{1}{2}(C_{11} + C_{66})K^2 \end{vmatrix} \tag{8.84}$$

This equation has the roots

$$\omega^2\rho = \frac{1}{2}(C_{11} + C_{12} + 2C_{66})K^2; \quad \omega^2\rho = \frac{1}{2}(C_{11} - C_{12})K^2 \tag{8.85}$$

How do we determine the direction of particle displacement? The first root when substituted into the upper equation of (8.44) gives

$$\frac{1}{2}(C_{11}+C_{12}+2C_{66})K^2u = \frac{1}{2}(C_{11}+C_{66})K^2u+\frac{1}{2}(C_{12}+C_{66})K^2v, \quad (8.86)$$

whence the displacement components satisfy $u = v$. Thus the particle displacement is along [110] and parallel to the $\boldsymbol{K}$ vector (Fig. 8.7). The second root of (8.20) when substituted into the upper equation of (8.44) gives

$$\frac{1}{2}(C_{11}-C_{12})K^2u = \frac{1}{2}(C_{11}+C_{44})K^2u+\frac{1}{2}(C_{12}+C_{44})K^2v, \quad (8.87)$$

whence $u = -v$. The particle displacement is along $[1\bar{1}0]$ and perpendicular to the $\boldsymbol{K}$ vector.

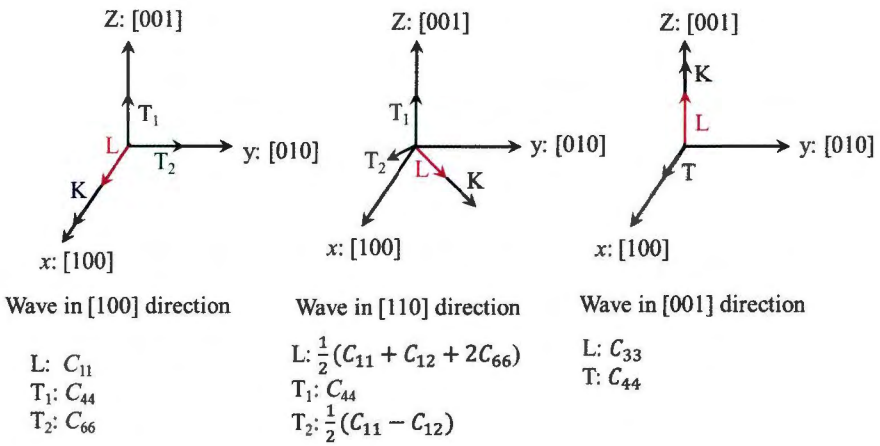

Figure 8.7: (Color online) Effective elastic constants for the three modes of elastic waves in the principal propagation directions in tetragonal crystals.

Bibliography

[1] Kamihara, Y., Watanabe, T., Hirano, M. Hosono, J. Am. Chem. Soc. 130, 3296 (2008).

[2] H. Takahashi, K. Igawa, K. Arii, Y. Kamihara, M. Hirano, and H. Hosono, Nature 453 (2008) 376.

[3] G. F. Chen, Z. Li, D. Wu, G. Li, W. Z. Hu, J. Dong, P. Zheng, J. L. Luo, and N. L. Wang, Phys. Rev. Lett. 100, 247002 (2008).

[4] Jiun-Haw Chu, James G. Analytis, Chris Kucharczyk, and Ian R. Fisher, PHYSICAL REVIEW B 79, 014506 (2009).

[5] Z.-A. Ren, J. Yang, W. Lu, W. Yi, X.-L. Shen, Z.-C. Li, G.-C. Che, X.-L. Dong, L.-L. Sun, F. Zhou, and Z.-X. Zhao, EPL (Europhysics Letters) 82, 57002 (2008).

[6] Z.-A. Ren, W. Lu, J. Yang, W. Yi, X.-L. Shen, Z.-C. Li, G.-C. Che, X.-L. Dong, L.-L. Sun, F. Zhou, and Z.-X. Zhao, Chinese Physics Letters 25, 2215 (2008).

[7] B. C . Sales, A. S. Sefat, M. A. McGuire, R. Y. Jin and D. Mandrus, phys. Rev. B79 (2009) 094521.

[8] H. Ogino, Y. Shimizu, K. Ushiyama, N. Kawaguchi, K. Kishio, and J. Shimoyama, Appl. Phys. Express 3 (2010) 063103.

[9] X. Wang, Q. Liu, Y. Lv, W. Gao, L. Yang, R. Yu, F. Li, and C. Jin, Solid State Communications 148, 538 (2008).

[10] F.-C. Hsu, J.-Y. Luo, K.-W. Yeh, T.-K. Chen, T.-W. Huang, P. M. Wu, Y.-C. Lee, Y.-L. Huang, Y.-Y. Chu, D.-C. Yan, and M.-K. Wu, Proceedings of the National Academy of Sciences 105, 14262 (2008).

[11] H. Ogino, Y. Matsumura, Y. Katsura, K. Ushiyama, S. Horii, K. Kishio, and J, Shimoyama, Supercond. Sci. Technol. 22, 075008 (2009).

[12] M. Rotter, M. Tegel, and D. Johrendt, Phys. Rev. Lett. 101, 107006 (2008).

[13] J. Paglione and R. L. Greene, Nature Physics 6, 645 (2010).

[14] S. Nandi, M. G. Kim, A. Kreyssig, R. M. Fernandes, D. K. Pratt, A. Thaler, N. Ni, S. L. Bud'ko P. C. Canfield, J. Schmalian, R. J. Mc-Queeney, and A. I. Goldman, Phys. Rev. Lett. 104, 057006 (2010).

[15] M. G. Kim, R. M. Fernandes, A. Kreyssig, J. W. Kim, A. Thaler, S. L. Bud'ko, P. C. Canfield, R. J. McQueeney, J. Schmalian, and A. I. Goldman, Phys. Rev. B 83, 134522 (2011).

[16] C. R. Rotundu and R. J. Birgeneau, Phys. Rev. B 84, 092501 (2011).

[17] N. D. Mathur, F. M. Grosche, S. R. Julian, I. R. Walker, D. M. Freye, R. K. W. Haselwimmer, G. G. Lonzarich, Nature 394 (1998) 39.

[18] E. Slooten, T. Naka, A. Gasparini, Y. K. Huang, and A. de Visser, Phys. Rev. Lett. 103 (2009) 097003.

[19] S. Doniach: in Valence Instabilities and Related Narrow-Band Phenomena, ed. R. D. Parks (Plenum, New York, 1977) p.169.

[20] M. Rotter, M. Pangerl, M. Tegel, D. Johrendt, Angew. Chem. 47, 7949 (2008).

[21] N. Ni, M. E. Tillman, J.-Q. Yan, A. Kracher, S. T. Hannahs, S. L. Budko, P. C. Canfield, Phys. Rev. B 78, 214515 (2008).

[22] S. Jiang, H. Xing, G. Xuan, C. Wang, Z. Ren, C. Feng, J. Dai, Z. Xu and G. Cao, J. Phys.: Condens. Matter 21 382203 (2009).

[23] S. A. J. Kimber, A. Kreyssig, Y.-Z. Zhang, H. O. Jeschke, R. Valent, F. Yokaichiya, E. Colombier, J. Yan, T. C. Hansen, T. Chatterji, R. J. McQueeney, P. C. Canfield, A. I. Goldman, D. N. Argyriou, Nature Mat. 8, 471 (2009).

[24] See the references in [19].

[25] M. A. McGuire, A. D. Christianson, A. S. Sefat, B. C. Sales, M. D. Lumsden, R. Jin, E. A. Payzant, D. Mandrus, Y. Luan, V, Keppens, V, Varadarajan, J. W. Brill, R. P. Hermann, M. T. Sougrati, F. Grandjean, G. J. Long, "Phase transitions in LaFeAsO: Structural, magnetic, elastic, and transport properties, heat capacity and Mössbauer spectra", phys. rev. B 78, 094517 (2008).

[26] R. M. Fernandes, L. H. VanBebber, S. Bhattacharya, P. Chandra, V. Keppens, D. Mandrus, M. A. McGuire, B. C. Sales, A. S. Sefat, and J. Schmalian, phys. rev. lett. 105 (2010) 157003.

[27] M. YOSHIZAWA, D. KIMURA, T. CHIBA, S. SIMAYI, Y. NAKANISHI, K. KIHOU, C. LEE, A. IYO, H. EISAKI, M. NAKAJIMA, and S. UCHIDA, "Structural Quantum Criticality and Superconductivity in Iron-Based Superconductor $Ba(Fe_{1-x}Co_x)_2As_2$", J. Phys. Soc. Jpn 81 (2012) 024604.

[28] T. GOTO, R. KURIHARA, K. ARAKI, K. MITSUMOTO, M. AKATSU, Y. NEMOTO, S. TATEMATSU, and M. SATO, J. Phys. Soc. Jpn 80 (2011) 073702.

[29] S. L. Bud'ko, N. Ni, S. Nandi, G. M. Schmiedeshoff, and P. C. Canfield, Thermal expansion and anisotropic pressure derivatives of Tc in $Ba(Fe_{1-x}Co_x)_2As_2$ single crystals, Phys. Rev. B 79, 054525 (2009).

[30] F. Hardy, P. Adelmann, T. Wolf, H. v. Lohneysen, and C. Meingast, Large anisotropic uniaxial pressure dependencies of T_{sc} in single crystalline $Ba(Fe_{0.92}Co_{0.08})_2As_2$ Phys. Rev. Lett. 102 (2009) 187004.

[31] S. Drotzinger, P. Schweiss, K. Grube, T. Wolf, P. Adelmann, C. Meingast, and H. v. Löhneysen: J. Phys. Soc. Jpn. **79** (2010) 124705.

[32] L. R. Testerdi and T. B. Bateman: Phys. Rev. 154 (1967) 402.

[33] T. Suzuki, H. Goshima, S. Sakita, T. Fujita, M. Hedo, Y. Inada, E. Yamamoto, Y. Haga, and Y. Onuki: J. Phys. Soc. Jpn. 65 (1996) 2753.

[34] Y. Yanagi, Y. Yamakawa, and Y. O no: Phys. Rev. B 81 (2010) 054518.

[35] M. Yoshizawa, I. Shirotani, and T. Fujimura: J. Phys. Soc. Jpn. 55 (1986) 1196.

[36] B. Luthi: Physical Acoustics in the Solid State (Springer, Heidelberg, 2004) p. 159.

[37] P. C. Canfield, S. L. Budko, N. Ni, J. Q. Yan, and A. Kracher: Phys. Rev. B 80 (2009) 060501(R).

[38] N. Doiron-Leyraud, P. Auban-Senzier, S. R. de Cotret, C. Bourbonnais, D. Jerome, K. Bechgaard, and L. Taillefer: Phys. Rev. B 80 (2009) 214531.

[39] S. Kasahara, T. Shibauchi, K. Hashimoto, K. Ikada, S. Tonegawa, R. Okazaki, H. Shishido, H. Ikeda, H. Takeya, K. Hirata, T. Terashima, and Y. Matsuda: Phys. Rev. B 81 (2010) 184519.

[40] Y. Onuki, R. Settai, K. Sugiyama, T. Takeuchi, T. C. Kobayashi, Y. Haga, and E. Yamamoto: J. Phys. Soc. Jpn. 73 (2004) 769.

[41] Y. Nakai, T. Iye, S. Kitagawa, K. Ishida, H. Ikeda, S. Kasahara, H. Shishido, T. Shibauchi, Y. Matsuda, and T. Terashima: Phys. Rev. Lett. 105 (2010) 107003.

[42] N. D. Mathur, F. M. Grosche, S. R. Julian, I. R. Walker, D. M. Freye, R. K. W. Haselwimmer, and G. G. Lonzarich: Nature 394 (1998) 39.

[43] Jiun-Haw Chu, James G. Analytis, Chris Kucharczyk, and Ian R. Fisher: Phys. Rev. B 79 (2009) 014506.

[44] S. L. Bud'ko, N. Ni, S. Nandi, G. M. Schmiedeshoff, and P. C. Canfield: Phys. Rev. B 79 (2009) 054525.

[45] T. Simizu, N. Yoshimoto, Y. Nakanishi, M. Yoshizawa: Physica. B **378-380** (2006) 407-408

[46] M. Saint-Paul, A. Abbassi, Z. S. Wang, H. Luo, X. Lu , C. Ren, H. H. Wen, and K. Hasselbach: Physica C **483** (2012) 207.

[47] V. Müller, Ch. Roth, D. Maurer, E. W. Scheidt, and K. Lüders: Phys. Rev. Lett. **58** (1987) 1224

[48] B. Golding, D. J. Bishop, B. Batlogg, W. H. Haemmerle, Z. Fisk, J. L. Smith, and H. R. Ott: Phys. Rev. Lett. **55** (1985) 2479.

[49] K. Miyake, and C. M. Varma: Phys. Rev. Lett. **57** (1986) 1627.

[50] R. D. Williams, and I. Rudnick: Phys. Rev. Lett. **25** (1970) 276.

[51] P. B. Littlewood, and C. M. Varma: Phys. Rev. B 26 (1982) 4883.

[52] S. Kondo *et al.*, Phys. Rev. Lett. 78, 3729 (1997).

[53] C. Pinettes and C. Lacroix, J. Phys. Condens. Matter, 6, 10093 (1994).

[54] H. R. Naren, A. Tamizhavel, S. Ramakrishnan and A. K. Nigam, Phys. Rev. Lett. 102 (2009) 187004.

[55] H. R. Naren, Arumugam Thamizhavel, Sushil Auluck, Rajendra Prasad, S. Ramakrishnan, arXiv:1011.4809v2 [cond-mat.supr-con] 13 Oct 2011

[56] M. Yoshizawa, D. Kimura, T. Chiba, S. Simayi, Y. Nakanishi, K. Kihou, C. H. LEE, A. Iyo, H. Eisaki, M. Nakajima, and S. Uchida

[57] Rikio Settai, Keisuke Katayama, Hiroshi Muranaka, Tetsuya Takeuchi, Arumugam Thamizhavel, Ilya Sheikin, Yoshisicko Onuki, Physics and Chemistry of Solids.71 (2010) 700.

[58] L. R. Testerdi and T. B. Bateman: Phys. Rev. 154 (1967) 402.

[59] T. Suzuki, H. Goshima, S. Sakita, T. Fujita, M. Hedo, Y. Inada, E. Yamamoto, Y. Haga, and Y. O nuki: J. Phys. Soc. Jpn. 65 (1996) 2753.

[60] S. Drotzinger, P. Schweiss, K. Grube, T. Wolf, P. Adelmann, C. Meingast, and H. v. Löhneysen: J. Phys. Soc. Jpn. **79** (2010) 124705.

[61] C. H. Lee, A. Iyo, H. Eisaki, H. Kito, M. T. Fernandez-Diaz, T. Ito, K. Kihou, H. Matsuhata, M. Braden, and K. Yamada: J. Phys. Soc. Jpn. **77** (2008) 083704.

[62] H. Usui and K. Kuroki: Phys. Rev. B **84** (2011) 024505.

[63] K. Kuroki: Solid State Commun. **152** (2012) 711.

[64] T. Saito, S. Onari, and H. Kontani: Phys. Rev. B **82** (2010) 144510.

[65] , K. Ahilan, T. Imai, A. S. Sefat, M. A. McGuire, B. C. Sales, D. Mandrus, P. Cheng, B. Shen, and H.-H. Wen: Phys. Rev. Lett. 104 (2010) 037001.